UNIUNEA EUROPEANĂ
Fondul Social European POSDRU 2007-2013
Instrumente Structurale 2007-2013
MINISTERUL EDUCAŢIEI ŞI CERCETĂRII ŞTIINŢIFICE
OIPOSDRU
Universitatea POLITEHNICA din Bucuresti

Proiect cofinanţat din Fondul Social European prin Programul Operaţional Sectorial Dezvoltarea Resurselor Umane 2007-2013
Investeşte în oameni!

Proiect InnoRESEARCH - POSDRU/159/1.5/S/132395
Burse doctorale şi postdoctorale în sprijinul inovării şi competitivităţii în cercetare

---

UNIVERSITY **POLITEHNICA** OF BUCHAREST
Faculty of Electrical Engineering
Doctoral School of Electrical Engineering

DOCTORAL THESIS SUMMARY

Accumulation and Effects of Space Charge in DC Cable Joints Insulations

Acumularea si Efectele Sarcinii Spatiale in Izolatiile Jonctiunilor Cablurilor de CC

Author: **M.Eng. Lucian-Viorel ŢĂRANU**

Supervisor: **Prof. Dr. Eng. Petru V. NOŢINGHER**

Bucharest
2021

Table of contents

Acknowledgements

I would like to thank, first of all, Prof. Petru V. Noțingher (doctoral advisor) for the support given throughout the elaboration of the doctoral thesis, for the recommendations, the countless discussions and all the offered advice and encouragement, especially in the last period working on the thesis. I am deeply grateful to him for all the time and interest given over the years.

I am also deeply grateful to Assoc. Prof. Cristina Stancu for all the discussions and support given throughout my thesis, as well as in the research project PN-II-RU-TE-2014-4-0280, respectively "Reduction of space charge in composite insulations of high voltage DC cables".

I express my deepest appreciation to my Doctoral Thesis Commission, respectively to Prof. Elena Helerea, Prof. Romeo Cristian Ciobanu and Assoc. Prof. Cristina Stancu for their efforts to analyse the thesis and for the suggestions offered in order to improve the thesis. I would also like to thank Prof. Emil Cazacu for accepting and presiding over the thesis defense.

Many thanks to Professors Laurențiu Marius Dumitran and Florin Ciuprina for the assistance offered throughout my thesis and for the discussions regarding the thesis contents.

I am extremely grateful to Prof. Gian Carlo Montanari from the University of Bologna for the chance to work alongside the LIT team (now LIMES) (Bologna) and for the important discussions regarding space charge. My deepest gratitude and thanks are also extended to Prof. Davide Fabiani (Director of LIT/LIMES) for his support, understanding and availability during my time at LIT, for the discussions on space charge, as well as for the provided technical support for space charge and microscopy measurements. I also wish to thank Dr. Fabrizio Palmieri for the discussions on the theory of space charge and its determination by PEA, the technical support for the experimental determination of space charge and electrical conductivity.

Special thanks to Dr. Fabrizio Negri for his friendship, discussions regarding space charge measurements and help regarding software for acquiring and processing space charge.

I also wish to thank Prof. Andrea Cavallini for all the discussions regarding PDs, technical assistance regarding PD measurement setup and PD identification in flat samples and cables.

Thanks also to Prof. Vittorio Colombo and the CIRI-MAM team (Bologna) for the access to the SEM microscope and to Prof. Andrea Saccani of DICAM (Bologna) for the assistance provided for the SEM measurements and the discussion on the results obtained.

I thank the Engineer Antonel Pleșa, R&D Director at ICME ECAB (Cablel) Bucharest, for access to the ICME ECAB research laboratories, providing the necessary materials for the experimental part of the thesis, the direct support in manufacturing cylindrical samples (cables) with multi-layered insulation (EPR / XLPE) and for all the discussions on polymeric materials. Also, I thank the Engineer Ionel Ciobanu from Prysmian Group Romania (Slatina) for his direct support in manufacturing XLPE / PVC cylindrical samples and for the samples informations.

Many thanks to Prof. Radu Setnescu and Dr. Eduard Marius Lungulescu (INCDIE ICPE-CA, Bucharest), for performing DSC and FTIR measurements and for their interpretations.

Thanks to all the technicians from UPB, ICME ECAB and LIT, for the assistance offered in the manufacturing of the samples and the measurement setup, without which the realization of the experimental part of the thesis would not have been possible. I also thank Prof. Alexandru Mihail Morega and Ms. Elena Floricău (SDIE, UPB), as well as Ms. Gaby Vasile and Ms. Carmen Dumitru (MMAE, UPB) for their support throughout the development of the thesis.

Thanks to the students from LIT (Bologna) from 2015–2016 and fellow students at ELMAT (UPB) for their support in conducting my experiments and for discussions and their friendship.

Thanks to all those who supported me but who were, unfortunately, not included here.

Special thanks to my life partner Mariana Guțu and to my parents, Mircea Țăranu and Voica Țăranu, for their understanding, support and, especially, for their patience.

The work has been funded by the Sectoral Operational Programme Human Resources Development 2007 – 2013 of the Ministry of European Funds through the Financial Agreement POSDRU/159/1.5/S/132395.

Introduction

The global economic increase is, currently, about +3.5 % per year, correlating in the latest years with an average global consumption of electrical energy of about +2.5 % per year. Due to these significant annual increases in electricity consumption, it is desired that its transmission and distribution be as efficient as possible, resulting in active research in the field to bring improvements to electricity transmission lines, so that they can withstand a voltage as high as possible in operation and to transport an electric power as high as possible.

The interest in cables for DC energy transport is observed, in recent years, by the emphasis on the development of DC technology [15] (currently, electrical networks using DC cables at voltages up to +/- 640 kV and power rating up to 3000 MW are commercially available [16]) as well as its integration into current AC networks. Considering that, currently, renewable energy sources represent over 80 % of the types of new energy sources installed in Europe (mostly wind energy) and the fact that in the future it is expected that renewable sources will have, globally, a share of at least 40 % of total energy sources, the transport of electricity in DC by cables is the most suitable avenue of transport.

The current trend of cable manufacturers is to use new technological processes to improve the purity of the polymeric material most often used for extruded type insulation, respectively polyethylene [16], but also to use new thermoplastic materials that do not require cross-linking and that have recyclability properties [34]. The thesis presents the results obtained on materials corresponding only to extruded insulation.

Because the cable sections have a finite length (usually less than 1 km), multiple cable sections have to be joined together in order to cover long distances. These are connected via cable joints. The cable joint is defined as the physical assembly that completely connects two (or more) cables together [40].

Cable joints for high voltage cables have a more complicated structure than the respective cables, the most vulnerable component of which is insulation. For higher distances, voltages and transported power, in recent years great efforts have been made to fabricate cable joints with insulations of polymeric materials, generally consisting of two polymer layers, usually between cross-linked polyethylene – XLPE, ethylene propylene rubber – EPR, ethylene propylene diene monomer rubber – EPDM or silicone rubber – SiR.

Space charge accumulation has been studied extensively in cables with extruded insulation and less in their joints, although cable accessories (their joints and terminals) are considered to be the most vulnerable parts of an electricity transmission network using cables. Thus, more precise measurements of space charge developed in the polymeric insulation of cables have been a subject of numerous research groups from universities and research centers. These researches culminated, in 2017, with the publication by the Technical Committee of the IEEE DEIS society of the first standard (IEEE 1732) which presents the protocol for performing space charge measurements in DC for materials used for extruded insulation of power cables, up to voltages of 550 kV [57].

For this (timely) research topic, the next step is to continue the studies on the accumulation of space charge for cable accessories ([30], [46]), materializing, in the end, with the publication of a standard similar to IEEE 1732 but for cable accessories.

The thesis supports the above goal, and in order to do so the thesis sets forth **three objectives (goals)** to follow and **four hypotheses** to investigate.

The thesis is structured in two parts and contains 9 chapters; the first part (the first 5 chapters, approx. 60 pages) contains the literature review and the second part (the following 4 chapters, approx. 140 pages) contains the original contributions and the conclusions.

In **Chapter 1** are presented an introduction to the topic, as well as the objectives pursued in this doctoral thesis.

In **Chapter 2** are presented informations on extruded insulated cable joints. The Chapter describes the structure of a cable joint, the materials used in the insulation layers, the types of cable joints and the differences between the cable joints used in AC and those in DC.

In **Chapter 3** are presented the stresses that can act on the extruded insulation of the cable joints, in operation. The Chapter discusses the thermal, electrical and other types of stresses that intervene and that generate or intensify the process of accumulation of space charge, having as effect the degradation of the cable joints.

In **Chapter 4** are discussed the mechanisms of DC conduction and electrical polarization, respectively the methods for determining the electrical conductivity (σ) and the electrical permittivity (ε).

In **Chapter 5** is treated extensively the problem of space charge in cable insulation and cable joints, describing the mechanisms of space charge injection and transport, as well as methods of measuring space charge. Of these, the PEA method is presented in more detail.

In **Chapter 6** are presented the materials, the measurement conditions and the measuring installations utilized in the thesis.

In **Chapter 7** are presented the experimental results regarding accelerated thermal ageing of the samples, the shape of the interface for the layered samples (obtained by microscopy) and the influence of working parameters (electrical voltage during the measurement, temperature applied during the measurement and ageing time) on the properties of studied materials: electrical conductivity, electrical permittivity and density of space charge.

In **Chapter 8** are presented the numerical results obtained for the distribution of the electric field for flat and cylindrical multi-layered structures (modelling the cable joint insulation) and for a cable joint design, using as input data the values obtained experimentally (permittivity, conductivity and density of space charge) in **Chapter 7**.

In **Chapter 9** are presented the general conclusions of the thesis, the personal contributions regarding the distribution and the effects of the space charge in the insulations of DC cable joints and the perspectives for the future.

The objectives of the thesis are:

- **O1.** Study the accumulation of space charge and determine its distribution in the insulation of power cable joints
- **O2.** Study the effects of space charge, respectively the resulting electric stresses, under the action of different electric and thermal stresses
- **O3.** Determine methods for reducing space charge

To pursue the above thesis objective, the following hypotheses were investigated:

- **H1.** Thermal ageing duration has a negative effect on the long term electrical properties of cable joint insulations, which in turn will negatively influence space charge values
- **H2.** Thermal ageing duration has a direct long term negative effect on the accumulation and distribution of space charge in cable joint insulations
- **H3.** The main effect of space charge is increased electrical stresses, that leads to cable joint insulation degradation
- **H4.** Both the reduction of space charge and its effects in cable joint insulations can be achieved by improved insulation manufacturing quality and improved cable joint design

In order to test the above hypotheses and pursue the thesis goals, measurements were performed on both flat and cylindrical samples (essentially a cable design with multi-layered insulation), unaged and thermally aged. Single-layer flat samples of XLPE, EPR, EPDM and multi-layered flat samples of XLPE / EPR and XLPE / EPDM were manufactured at ICME ECAB (Cablel), Romania. The cylindrical geometry cable samples with EPR / XLPE insulation were manufactured by ICME ECAB (Cablel) Romania.

The values of the electrical properties of the components that form the multi-layered insulation of a DC cable joint (electrical conductivity and permittivity, dielectric loss factor, level of partial discharges and density of space charge) were measured. The variations of these properties and of other chemical and morphological changes were followed during laboratory accelerated thermal ageing for a period of up to 90 days.

The determination of the electrical permittivity and the loss factor was obtained by dielectric spectroscopy in the Laboratory of Electrotechnical Materials (ELMAT) at University Politehnica of Bucharest (UPB), Romania. The determination of the electrical conductivity was obtained by the method of absorption and resorption currents at the Laboratory of Innovation Technology (LIT) (now LIMES), Bologna, Italy, and at ELMAT, UPB, Romania. The volume charge density was determined by measurements using the PEA method at LIT in Bologna, Italy. Sample degradation was determined by Fourier transform infrared spectroscopy (FTIR) and Differential scanning calorimetry (DSC) at the National Research and Development Institute for Electrical Engineering (INCDIE ICPE-CA), Romania. The interface shape of the flat layered samples was determined by the method of optical microscopy (OM) at ELMAT and by the method of Scanning electron microscopy (SEM) at the Center for Industrial Research (CIRI), Bologna, Italy, on samples prepared at the Department of Civil Engineering, Chemistry and Environment (DICAM), Bologna, Italy, and gold sputtered at LIT.

Chapter 1. Introduction

In Chapter 1 is presented an introduction to the topic (a summary of which was presented above), as well as the objectives and hypotheses pursued in this doctoral thesis.

The importance of electrical energy transport is highlighted, based on the current and future electricity needs of the world, in fig. 1. The differences of high voltage alternating current (HVAC) and direct current (HVDC) technologies and the advantages of HVDC using cables for energy transport are discussed. The components of a power cable are presented, highlighting the insulation layer and presenting various types of cable insulations and the advantages of extruded insulation. The concept of cable joints for joining two cables is introduced here, emphasizing on the interface area between cable and joint insulations.

In Chapter 1 is also provided a summary of the major problems that state of the art research is currently addressing, respectively the insulation stresses the cable joints are subjected to, including the dependence of electrical conductivity on the electric field values and temperature and the accumulation of space charge.

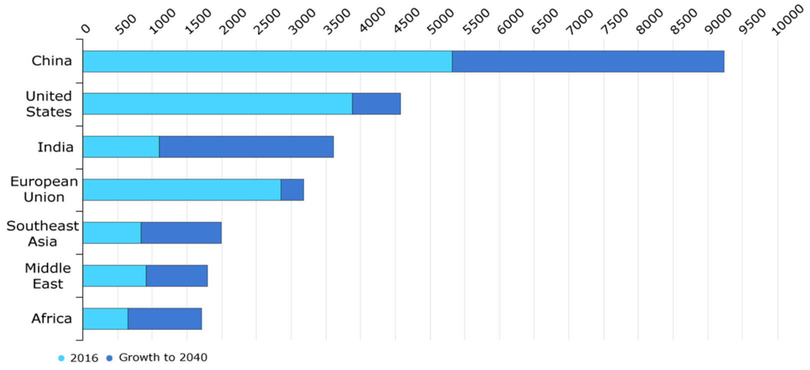

Fig. 1. Electricity demand by region, 2016 – 2040 [19]

Chapter 2. Power cable joints

In Chapter 2 are presented the functions of cable joints, their structure, types of cable joints with extruded insulation, the materials used in the insulation layers and the differences between cable joints used in AC and in DC.

The Chapter stresses the importance of development of reliable cable joints for extruded insulation cables, at electrical voltages and installed powers as high as possible [30]. Among the functions performed by a cable joint, the function of control of electric stresses is further discussed. Here, the method of using Field Grading Materials (FGM) for stress-control is described and is shown to be efficient.

The Chapter also presents a classification of joints based on type and the particularities of each type and the voltage levels it is installed for. Among these, the most installed type of joint for HVDC has been identified to be the premoulded prefabricated joint, and is the type of joint considered in the thesis. The constructive elements of a one-piece premoulded prefabricated joint is presented in fig. 2, highlighting the interface area (fig. 2, B) between the cable insulation layer (fig. 2, C) and the cable joint insulation layer (fig. 2, A).

Ethylene propylene rubber (EPR), Ethylene propylene diene monomer rubber (EPDM) and Silicone rubber (SiR) have been identified as materials which are used for the insulation layer of prefabricated joints, with EPR and EPDM more common in HVDC and SiR in HVAC. Moreover, the growing interest for SiR for HVDC cable joints insulations is discussed.

The conclusions of Chapter 2 are:

- An effective method of controlling electric stresses in DC joint insulations is by employing Field Grading Materials, and was pursued in relation to Hypothesis H4 regarding reducing space charge and its effects by improved cable joint design.
- Both EPR and EPDM have been identified as most used joint insulation materials for power transmission in DC using premoulded prefabricated joints, and are used in the thesis.
- A study regarding which type of material is most suitable for cable joint insulations in contact with cable insulation (XLPE) was pursued in relation to Hypothesis H4 regarding reducing space charge and its effects by improved cable joint manufacturing quality.

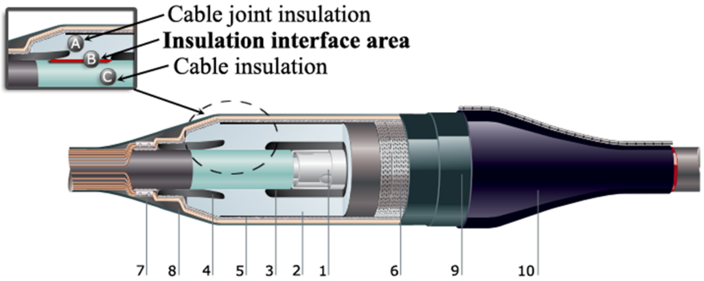

Fig. 2. One-piece premoulded joint, for a nominal voltage of 245 kV:
1- mechanical connector; 2- silicone rubber insulation body; 3- inner electrode;
4- deflector; 5- external semiconductive screen; 6- Copper braid; 7- screen connection;
8- mastic; 9- insulation tubes; 10- external protection [92], highlighting the insulation interface area (B) between the cable insulation (C) and the cable joint insulation (A)

Chapter 3. Stresses for DC cable joints extruded insulations

This Chapter presents the stresses that can act on the extruded insulation of the cable joints in operation, the lifetime of their insulation being determined by their behaviour under the action of these various stresses [73]. The electrical, thermal, mechanical and environmental stresses that intervene and that generate or intensify the process of accumulation of space charge, having as effect the degradation of the cable joints, are discussed.

The electrical stresses and their effects include Partial discharges (PD), Electrical and electrochemical trees and, especially, Space charge. The space charge (generated from the manufacturing process or from the operation of the joint) influences the distribution of the electric field, both during the application of voltage, as well as after removing the voltage (where it can endanger cable technicians). The existence of space charge also leads to the appearance / intensification of partial discharges and electric trees, increasing the electric stresses and leading to a premature degradation of the joint insulation. Figure 3 summarizes the action of electrical stresses on the insulation system of cable joints.

Among the thermal stresses acting on the insulation system of the joint, thermal ageing was discussed, showing that it leads to the formation of free radicals which, through successive reactions, causes the cleavage of molecular chains and the appearance of oxidation products [172]. This can be slowed by introducing antioxidants into the insulation materials (XLPE, EPDM, EPR, etc.) in the cable joint's insulation structure. The section concludes that thermal ageing of cable joints involves two main pathways: continuous changes of the chemical and physical structure of the insulation of the cable joint due to chemical degradation, polymerization and depolymerisation, diffusion etc., and thermo-mechanical effects caused by the forces generated by expansion and contraction phenomena.

The rest of Chapter 3 presents the most common mechanical and environmental stresses and discusses their effects on the cable joint insulation.

The conclusions of Chapter 3 are:

- In the case of cable joint insulation, most types of stresses will increase the density of space charge (including partial discharges, electrical trees, the presence of additives or impurities, delamination due to thermal or mechanical stresses, etc.) which will in turn change the distribution of the electric field in the insulation layers of the joint, and will lead to accelerated electrical (or thermoelectric) ageing, local degradation and breakdown.
- The literature reviewed in this chapter indicated that a major effect of space charge is increased electrical stresses which leads to cable joint insulation degradation, which supports the Hypothesis H3. Moreover, it has been shown that thermal ageing has a negative effect on electrical properties of cable joint insulation materials (supporting Hypothesis H1) and on space charge accumulation (supporting Hypothesis H2).

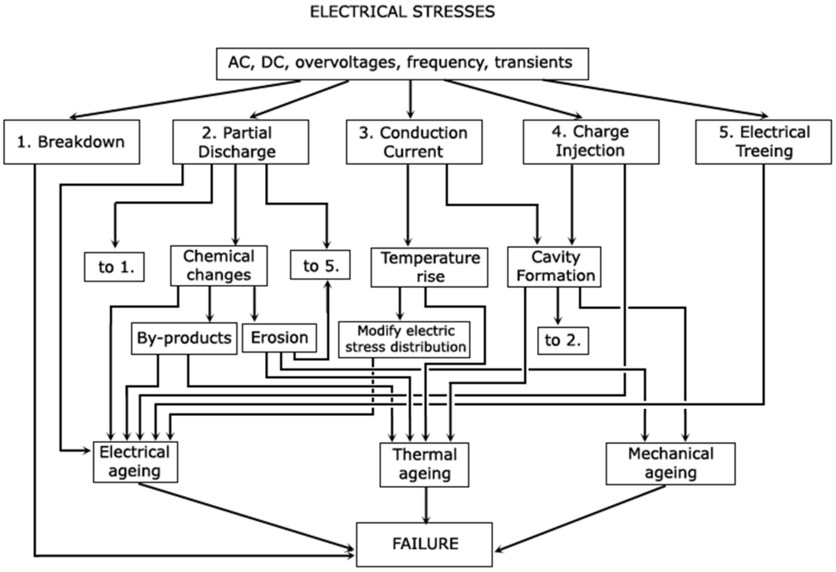

Fig. 3. The action of electrical stresses on the insulation system of cable joints [132]

Chapter 4. Electrical conduction in DC joints insulations

In Chapter 4 the mechanisms of DC conduction and electrical polarization, respectively the methods for determining the electrical conductivity (σ) and permittivity (ε) are analysed.

The electrical conduction in the insulations of the cable joints depends on the morphology of the material and the nature, concentration and mobility of the charge carriers, respectively the ions (of impurity, additives, etc.) and electrons / voids.

Ionic conduction is highlighted to be present in cable joints insulations, and its mechanisms are presented over various temperatures and electric field values (from usual to high temperatures and from low to high, respectively over 100 kV/mm, electric field values).

Electronic conduction is also highlighted to be present in cable joints insulations, both in low and medium electric fields ($E < 10^7$ V/m), and in high electric fields ($E > 10^7$ V/m). For low and medium electric fields the existence of traps is discussed, offering a classification of traps in shallow traps (< 0.6 eV, corresponding to defects in the molecular structure of the polymer) and deep traps (> 1 eV, corresponding to chemical irregularities in the polymer) [200].

It is discussed that these localized states (traps) are places where the charge carriers can be captured; if a charge carrier (e.g. an electron) is trapped, it cannot get out unless it receives sufficient energy, equal to the depth of the trap or equal to the difference between the current and the neighbouring trap. The existence of traps capturing charge carriers generally reduces the concentration of carriers that can participate in the conduction process, or reduces their mobility, causing local accumulations of space charge that produce a local electric field that, in addition to the electric field produced by the applied voltage, may cause premature degradation of the material.

For the electronic conduction in high electric fields it was shown that, besides the presence and the intensification of the phenomena that appear in low and medium electric fields, under the action of higher electric fields there are new mechanisms that are limited (or controlled) by the electrodes (charge injection at the interface between the dielectric and the electrode) and by the bulk of the insulation (charge migration inside the material). Their consequence is a premature ageing or a local degradation of the material.

Among the charge injection mechanisms, the Schottky and the Fowler-Nordheim injections are treated in more detail, offering values for the expressions of their current densities. Among the charge transport mechanisms, the Poole-Frenkel effect, the Hopping conduction and the Space charge limited conduction are presented in more detail, offering values for the expressions of their current densities or conductivities.

The determination of the electrical conductivity (which characterizes the state of electrical conduction) can be performed using empirical methods, via different computation formulas, or experimentally, using the method of absorption-resorption currents.

For the empirical determination, various formulas in which the conductivity depends on the values of the electric field and / or the temperature are presented. Among these, the expression in eq. (4.36) was proposed by the author and was later used in the thesis:

$$\sigma(E,T) = A \cdot \exp\left(-\frac{E_a}{k_B \cdot T}\right) \frac{\sinh\big((a \cdot T + b) \cdot \ln|E|\big)}{|E|^{\alpha}} \tag{4.36}$$

where A, E_a, a, b and α are material constants, k_B is Boltzmann's constant and T is the thermodynamic temperature.

For the experimental determination, the method of absorption-resorption currents (used in the thesis) is presented at length, and the electrical conductivity expression is deduced.

The determination of electrical permittivity (which characterizes the state of electrical polarization) is presented via the broadband dielectric spectroscopy method (employed in the thesis).

The conclusions of Chapter 4 are:

- The changes that the insulating material suffers during ageing can be reflected in the values of electrical conductivity. This supports Hypothesis H1 that claims that the thermal ageing has a negative effect on long term electrical properties of cable joint insulations.
- The electrical permittivity can be used as a marker for assessing the ageing state of the samples, pursuing Hypothesis H1 that claims that the thermal ageing duration has a negative effect on the long term electrical properties of the cable joint insulations.
- In cable joints, because there are discontinuity surfaces (interfaces) where electric charge separates (based on the ratio between permittivity and conductivity of each homogeneous part separated by the interface) a surface charge density can exist, which outputs an additional electric field. An increase of space charge due to the existence of surface charge density supports Hypothesis H1 that claims that the electrical properties changes induced by the thermal ageing will negatively influence the space charge values.

Chapter 5. Space charge

In Chapter 5 the problem of space charge in cable insulation and cable joints is treated extensively, describing the mechanisms of space charge injection and transport, as well as methods of measuring space charge. Of these, the PEA method is presented in more detail.

Space charge is defined here as the accumulation of free electric charges (which are likely to move) of positive and negative polarity, contained in a dielectric material without taking into account the electric charges of opposite polarities that cancel each other out [231]. The accumulated space charge depends on the chemical structure of the dielectric, temperature, applied electric field value, the measurement duration, the nature of the electrodes, etc.

The distribution of these space charges (fig. 4, *a*) modifies the distribution of the electric field E (fig. 4, *b*) by creating an additional internal electric field which, adding to the applied electric field E_{app} (defined as the ratio between the applied voltage, U_{app}, and the thickness of the sample, g), can lead, in certain areas, to a local electric field that is superior to the value for which the insulation was dimensioned, thus contributing to the acceleration of the insulation degradation processes, respectively to its premature breakdown [247].

Space charge is classified in extrinsic (injected from the electrodes) and intrinsic (generated by defects introduced by the manufacturing process or produced during operation) charge, and is further classified depending on where it accumulates in the dielectric, respectively in the vicinity of electrodes, in its bulk, at interfaces, etc.

The charges that accumulate in the vicinity of electrodes are further classified into homocharges and heterocharges. Charges of the same sign as the polarity of the voltage at the interface, accumulated over a distance Δx near the electrodes, are called *homocharges*, and show that the injection / extraction of the charge is the dominant mechanism. Their effect is decreasing the electric field towards the electrode and increasing it inside the sample.

Charges of opposite sign to the polarity of the voltage at the interface, accumulated over a distance Δx near the electrodes, are called *heterocharges* and have the effect of increasing the electric field at the dielectric – electrode interface and decreasing the electric field in the bulk of the sample. Heterocharges can be generated by the ionization of chemical species / impurities present in the sample, the dominant mechanism being the transport of electric charge.

Among various measurement methods for determining space charge, the pulsed electro-acoustic (PEA) method can be successfully used for flat and cylindrical samples, cables or cable joints [252]. It consists in the use of an excitation of electrical origin (short-term voltage pulses) that generates an acoustic pressure wave that propagates in the sample, determines a local displacement of the internal electrical charges present and is detected by a piezoelectric sensor. The shape of the signal in the external circuit depends on the distribution of the electric charge, and, via mathematical treatment, the space charge density distribution can be determined.

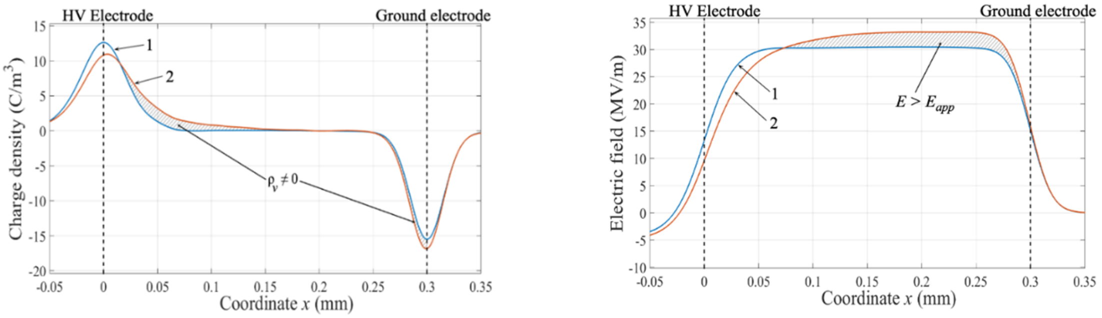

a) b)

Fig. 4. Variation of the space charge density (*a*) and the electric field (*b*) with the coordinate *x*, for flat XLPE samples, at t = 1 s (**1**) and 3600 s (**2**) after voltage application (E_{app} = 30 kV/mm)

As the results obtained for the distribution of the space charge differ depending on the order chosen for the Gaussian filter (from the mathematical treatment discussed above), Chapter 5 also presents the results of a study regarding the influence of the Gaussian filter order. Choosing an order for the Gaussian filter that is suitable for the deconvolution of all experimentally obtained signals is a challenge, among other things, due to the fact that the results also depend on the amplitude of the input electrical signal: a signal with a higher amplitude, either from a sample with more space charge or from a higher applied voltage, accepts a higher value of the filter order until high frequency components appear as a result of deconvolution, while the same order of the Gaussian filter but applied to a signal with a lower amplitude produces a result with many high frequency components which distorts the signal.

This study considered a range between 2 and 50 for the Gaussian filter order and studied its influence for samples of XLPE (g = 0.3 mm) and EPR (g = 0.5 mm) subjected to a low and a high applied electric field (E_{app} = 2 ... 10 kV/mm). The variation of the volume charge density for XLPE flat samples are presented in fig. 5 with distance in arbitrary units and with offset on the ordinate, and in fig. 6 at the ground electrode position with values relative to their maximum. Taking into account the loss of the resolution in the area of the high voltage electrode (see §5.2.5), the fact that the samples studied in the thesis have different acoustic properties (being, thus, different media, with both low and high electrical signal losses), that they were measured at both low and high voltage values and that the total electrical signal resolution when employing a Gaussian filter order of 5 is acceptable for all cases considered, this value for the order of the filter is chosen as the compromise value used for all the determinations by deconvolution of the electrical signal performed within the thesis.

As the electrical signal obtained after the application of the numerical treatment is variable over time and not in space, the calibration procedure for the space charge density results is presented, for both flat and cylindrical geometries.

As the acoustic waves are attenuated and dispersed as they pass through lossy mediums (such as the samples used in the thesis), the signal detected by a sensor positioned at one end of the sample does not correspond directly to the distribution in the sample. In fig. 7, the effects of attenuation and dispersion (fig. 7, curve **1**), compared to the ideal electrical signal (fig. 7, curve **2**), is presented for a XLPE sample (fig. 7, *a*) and an EPR sample (fig. 7, *b*). It is observed that the electrical signal is more attenuated and dispersed in samples that have a more amorphous chemical structure (EPR compared to XLPE).

The interface between the two layers in the case of multi-layered sample is an area where the electroacoustic wave suffers reflections, and a method to determine if the reflections interfere with the obtained result is presented.

There are two methods to measure space charge using PEA: under applied voltage (Voltage-ON) and in the absence of applied voltage (Voltage-OFF). The Voltage-ON measurements are for determining the distribution and dynamics of the volume space charge density over time, due to the injection of charge carriers and bulk charge displacement phenomena (previously discussed in Chapter 4), and Voltage-OFF measurements are for determining the density of space charge present in the sample in the absence of the high voltage source, captured in traps corresponding to physical and chemical irregularities.

For Voltage-OFF measurements, the term $\rho_{v,avg}$ is introduced as the residual charge density, or, the average (value of the volume) charge density, and is used to compare, from the point of view of space charge accumulation, different types of materials or even the same type of material but subject to different experimental conditions. It is computed by eq. (5.19) [261]:

$$\rho_{v,avg}\left(t_{0,Voff}\right) = \frac{1}{x_d - x_0 - 2 \cdot x_\delta} \cdot \int_{x_0+x_\delta}^{x_d-x_\delta} \left|\rho_v\left(t_{0,Voff}, x\right)\right| dx\,, \tag{5.19}$$

where $t_{0,Voff}$ represents a moment of the signal acquisition in the measurement mode Voltage-OFF (usually chosen between 1 ... 10 seconds after the beginning of the measurement in Voltage-OFF), x_0 and x_d represents the coordinate positions of the HV and ground electrodes and x_δ represents a distance equal to 3 % of the sample thickness, used to exclude from the calculations the values in the immediate vicinity of both electrodes.

There are errors when measuring space charge. Among those, Chapter 5 mentions approximation errors and signal detection errors. The approximation errors are generated by the user (measuring sample sizes etc.) and are generated by the sample's thickness compression when introduced in the measuring cell. The latter are determined to be higher (up to 15%) in the case of elastic samples (EPR and EPDM rubbers) and smaller (≈ 5 %) in the case of thermosetting samples (XLPE). These errors influence the real value of the electric field applied by the high voltage source. The errors due to the compression of samples were ignored, with their thickness determined when measuring the sample's dimensions (see Chapter 6).

Among the signal detection errors, besides the errors due to the finite width of the voltage pulse (affecting the resolution of the system) and the various electronic equipment in the acquisition system acting as low-pass filters (worsening the system resolution), those due to the attenuation and dispersion of the electrical signal (affecting differently each type of material due to different acoustic properties) and those due to the overlap of reflected waves over the desired signal (measurements on multi-layered samples) have been investigated. In the case of the results presented in the thesis, all the measurements were performed on the same equipment and following the same procedure, so that it is considered that the resolution of the system is the same for all the measurements. It was also determined that in the case of multi-layered samples of XLPE / EPR and XLPE / EPDM (see Chapter 6) where XLPE is connected to the HV electrode, the error caused by the overlap of the reflected waves over the desired signal is approx. 5 % and where EPR or EPDM are connected to the HV electrode is approx. 11 %.

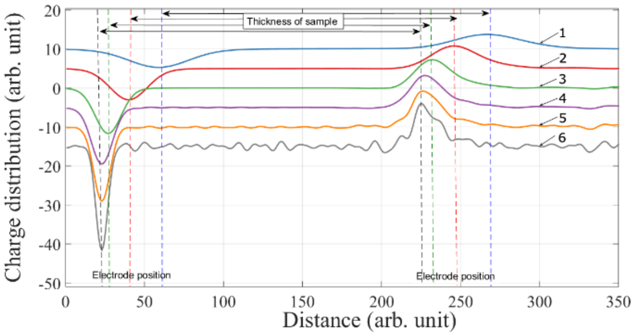

Fig. 5. Variation of the volume charge density for XLPE flat samples at a high applied field, in arbitrary units and with offset on the ordinate (...)

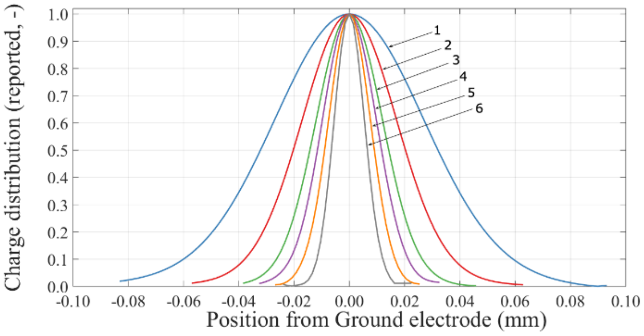

Fig. 6. Variation of the volume charge density (relative to its maximum value) for XLPE flat samples at the ground electrode area (...)

(...) → for Gaussian filter order: 2 (**1**), 5 (**2**), 10 (**3**), 15 (**4**), 25 (**5**), 50 (**6**)
(XLPE, t = 1 s after applying the voltage, E_{app} = 10 kV/mm)

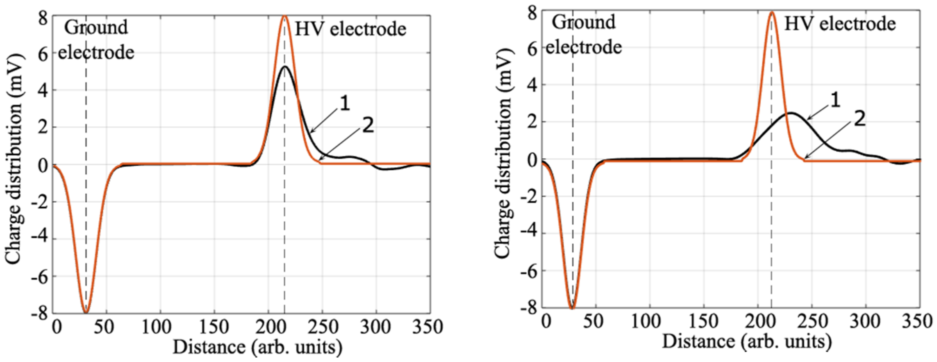

a) b)

Fig. 7. Attenuation and dispersion of the resulted electrical signal (**1**) compared to the ideal electrical signal (**2**) in the case of a XLPE sample (*a*) and EPR sample (*b*) (t = 1 s after applying the voltage, E_{app} = 5 kV/mm)

The conclusions of Chapter 5 are:

- The accumulated space charge changes the distribution of the electric field by creating an additional electric field that can lead to local intensifications that contribute to insulation degradation processes, supporting Hypothesis H3 regarding the effects of space charge.
- In the thesis, the volume charge density distribution is obtained from the measured electrical signal by using methods of numerical treatment on the signal, neglecting the effect of attenuation and dispersion and by calibrating the signal.
- For the numerical treatment of the signal, the order of the Gaussian filter was chosen as 5. This value, although chosen to be suitable for all measurements, has the disadvantage that it will disperse in space the electrical signal corresponding to the space charge on the surface between the electrode and sample (see curve **2** from fig. 6), overlapping, locally, with the electrical signal corresponding to the space charge in the vicinity of electrodes.
- The residual charge density can be used to highlight space charge accumulation for the same material but subjected to different measurement stresses or for different materials subjected to the same measurement stresses, and can be used to pursue Hypothesis H2 regarding quantifying the direct effect of thermal ageing on accumulation of space charge.

Chapter 6. Experiments

In Chapter 6 the samples, the measurement conditions and the measuring installations are presented.

6.1. Samples

Conducting research on flat or cylindrical multi-layered samples is typical for HVDC cable accessory design, and is well established in the literature if of interest is what happens at the cable joint's insulation area. Following the discussion of Chapter 2, the samples that represent the DC cable joint insulations that were used for experiments were manufactured at ICME ECAB Bucharest (flat and cylindrical samples). The flat multi-layered samples obtained from flat uni-layered samples follow the design of the insulation area of cable with extruded insulation – prefabricated premoulded cable joint (shown to be the most used type of cable joint in HVDC). The cylindrical samples follow more closely the design of the same insulation area, as they also include the cable conductor and inner semiconductive screen.

The flat samples were manufactured in the R&D Laboratory of ICME ECAB, on a GIBITRE Instruments laboratory press. The primary materials were low density polyethylene pellets and strips of unvulcanised ethylene propylene and ethylene propylene diene monomer rubbers. The flat samples were obtained in moulds of thickness h_{mould} = 0.3, 0.5 and 0.8 mm based on procedures developed after a significant number of tests at different values of temperature and pressure [262] and microscopic analysis of the samples to determine the quality of their surfaces, the existence of gaps, agglomerations, protuberances etc. (see section §7.1). Some of the resulting flat samples are presented in fig. 8. They were manufactured from a single material (uni-layered samples, fig. 8, *a*, *b* and *d*) and from two materials (multi-layered samples, fig. 8, *c* and *e*).

For manufacturing cross-linked polyethylene (XLPE) samples (fig. 8, *a*), low density cross-linkable polyethylene pellets, Borlink LE4201R were used, following the steps presented in Annex §A.1. The XLPE samples obtained in this way have a thickness of g = 0.30 mm and have relatively smooth surfaces, without obvious roughness. The standard deviation on the total number of manufactured XLPE samples is 0.004 mm, but the samples obtained were grouped into categories where the standard deviation of the group is below 0.002 mm.

Ethylene propylene rubber (EPR) samples (fig. 8, *b*) were obtained following the steps presented in Annex §A.2. They have a thickness of g = 0.50 mm and have relatively smooth surfaces, without obvious roughness. The standard deviation on the total number of manufactured EPR samples is 0.012 mm, but the samples obtained were grouped into categories where the standard deviation of the group is below 0.005 mm.

Ethylene propylene diene monomer rubber (EPDM) (g = 0.50 mm) samples (fig. 8, *d*) were obtained following the steps presented in Annex §A.2, the same as for the EPR samples.

XLPE / EPR multi-layered samples (fig. 8, *c*) were obtained following the steps presented in Annex §A.3. They have a thickness of g = 0.80 mm and a smooth interface area, in the form shown in section §7.1. The standard deviation on the total number of XLPE / EPR manufactured samples is 0.016 mm, but the samples obtained were grouped into categories where the standard deviation of the group is below 0.006 mm.

Manufacturing of XLPE / EPDM (g = 0.80 mm) multi-layered samples (fig. 8, *e*) follows the same steps as those for manufacturing XLPE / EPR multi-layered samples (§A.3).

The cylindrical samples represent models of DC cable joints and were manufactured by ICME ECAB with industrial equipment used in the manufacture of medium voltage cables. The samples consist of a multi-wire conductor (Aluminium) covered by an inner semiconductor screen layer and two insulation layers, named S_{in} (the layer over the conductor, ethylene propylene rubber (EPR)) and S_{out} (the outer layer of cross-linked polyethylene (XLPE)) (the outer cable semiconductor screen layer is, now, an insulation layer of XLPE).

The cylindrical samples structure is: a round multi-wire Aluminium conductor with a diameter of 14 mm over which was placed a semiconductor layer of polyethylene with carbon black (of thickness g_0 = 0.7 … 1 mm), the first insulation layer S_{in} – of ethylene propylene rubber (EPR) (of thickness g_1 = 3.3 … 3.7 mm) – and, after, the second insulation layer S_{out} – of cross-linked polyethylene (XLPE) (of thickness g_2 = 0.9 … 1.2 mm) (fig. 9).

In order to reduce (eliminate) the internal mechanical stresses and the content of by-products resulting from the technological manufacturing processes, all the samples were subjected, at UPB, to a thermal conditioning of 48 h at T = 50 °C, in a TRADE RAYPA laboratory oven with forced air circulation and adjustable temperature (between 30 and 250 °C).

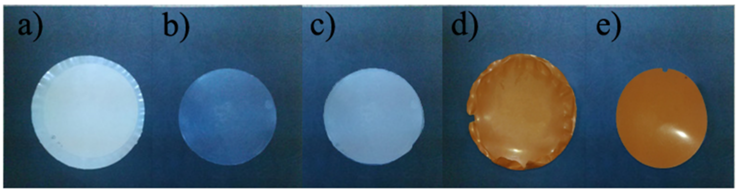

XLPE g = 0.3 mm

EPR g = 0.5 mm

XLPE / EPR g = 0.8 mm

EPDM g = 0.5 mm

XLPE / EPDM g = 0.8 mm

Fig. 8. Flat samples manufactured at ICME ECAB,
a) XLPE, b) EPR, c) XLPE / EPR, d) EPDM and e) XLPE / EPDM

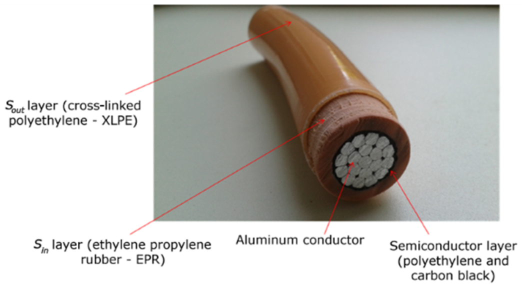

Fig. 9. EPR / XLPE cylindrical samples manufactured at ICME ECAB

6.2. Installations and measurement conditions

6.2.1. Differential scanning calorimetry (DSC)

Differential scanning calorimetry (DSC) measurements were performed (non-isothermally) with a Setaram 131 EVO equipment at INCDIE ICPE-CA. Mini-samples (3×3 mm^2) from all samples were measured, in the presence of air (flow rate of 50 ml/min). The temperature varied between 30 and 380 °C, with 4 growth rates: 2, 4, 6 and 10 °C/min.

The experimental results were processed using the Calisto Data Processing (CDP) software and the oxidation initiation temperature T_o was calculated according to the standard ASTM E2009-08. The minimum value in the set of maximum temperatures T_m corresponding to the exothermic oxidation reaction was used as the temperature limit for thermal ageing.

6.2.2. Thermal ageing

Thermal ageing of unaged samples (I0) was performed in a TRADE RAYPA laboratory oven with forced air circulation. The ageing temperature was chosen as 120 °C (see §7.2), and the thermal ageing times were 30 (noted with I1), 60 (noted with I2) and 90 days (noted with I3).

After ageing, the samples were transported to Bologna for space charge measurements. For the same baseline for comparison, the measurements were performed for all samples at 48 – 60 hours after removal from the laboratory oven. During this time it is possible that part of the degradation products to be neutralized and that the space charge density measured then to be different from that measured immediately after sample removal from the laboratory oven.

A study of the variation of space charge density (or the values of residual space charge) with the period of storage (the elapsed time between the end of accelerated ageing and the actual measurement) is an interesting perspective, but for the characterisation of the materials of the present study the measurement at the same elapsed time was sufficient.

6.2.3. Optical and scanning electron microscopy

The determinations by optical microscopy (OM) were performed in the Laboratory of Electrotechnical Materials (ELMAT) at UPB, on an Optical microscope at a 40 X magnification, on mini-samples of XLPE, EPR, EPDM, XLPE / EPR and XLPE / EPDM which have been prepared by sectioning layers with a microtome.

Determinations by electron scanning microscopy (SEM) were performed at CIRI, Bologna, on a Phenom ProX microscope. Mini-samples were taken from the multi-layered samples by inserting half of a manufactured sample in liquid nitrogen and sectioning into 1 cm^2 pieces immediately after removal from the liquid nitrogen bath (at DICAM, Bologna). The mini-samples thus obtained were fixed in a mount between two rectangular pieces of polyethylene and were metallized by a gold layer sputter deposited in vacuum at LIT, Bologna. The metallized mini-samples were introduced into the measuring box of the microscope with the EPR part on the left and the XLPE part on the right. SEM analysis was performed on the mini-samples by using the backscattered electron detector (BSD) at a voltage value of 10 kV.

6.2.4. Fourier transform infrared spectroscopy (FTIR)

The action of temperature on the polymeric material in the presence of air and air humidity leads to the formation of free radicals which, by successive reactions lead to the cleavage of the polymer chain and oxidation products, such as carbonyl, hydroxyl, unsaturated or acid groups grafted on the polymer chain [265].

The thermal ageing state of the samples was determined by Fourier-transform infrared spectroscopy (FTIR) on mini-samples of XLPE, EPR and EPDM. The infrared (IR) spectra of unaged and aged mini-samples were recorded with a Jasco 4200 spectrometer coupled with a JASCO PRO 470-H ATR accessory at INCDIE ICPE-CA.

The mini-samples were measured directly by placing them on the crystal of the ATR device and pressing with a controlled force, using the following spectrum recording conditions: spectral domain: 4000 – 400 cm^{-1} ; resolution: 4 cm^{-1} ; number of scans: 50 accumulations.

6.2.5. Electrical conductivity

The electrical conductivity of the flat samples was determined via the absorption / resorption current method and using the Keithley 6517B Electrometer equipment at LIT (Bologna) for high applied voltages and at ELMAT (Bucharest) for low applied voltages.

In the case of low voltage measurements, the samples were introduced into the RESISTIVITY Chamber 8009 cell of the Keithley 6517B Electrometer, without adhering electrode material. In the case of high voltage measurements, both sides for the measured samples were metallized by a gold layer sputter deposited in vacuum at LIT (Bologna) and they were introduced into a measuring cell specially manufactured at LIT, Bologna (fig. 10).

In order to characterize different materials at the same electric stresses (see Chapter 3), the study parameter *Applied electric field* (E_{app}) is introduced. Hereinafter, for both conductivity and space charge measurement results (presented thoroughly in Chapter 7) as well as for numerical computations (presented in Chapter 8), the applied electric field is defined as the ratio between the applied voltage on the sample and the sample's thickness.

The measurements conditions are summarized below:

- Temperature: 30 – 70 °C
- DC power supply, positive polarity
    - Low voltage: voltage source built into the Keithley 6517B
    - High voltage: F.u.G. Elektronik HCN 35-35000
- Applied electric field: 1 – 30 kV/mm
- Measurement duration: 1 hour absorption (i_a) and 1 hour resorption (i_r)

6.2.6. Electrical permittivity

Using the dielectric spectroscopy method (presented in Chapter 4), the dielectric properties of the flat samples were determined with a NOVOCONTROL dielectric spectrometer at ELMAT, Bucharest.

The measured flat mini-samples were discs (diameter D_{es} = 42 mm), for which adhering electrodes (diameter D_{el} = 40 mm) from copper foils complete with a semiconductor adhesive layer (3M Conductive Copper Foil Tape 3313) were placed on both sides of the sample.

Measurements were performed for frequencies f = 10 mHz … 1 MHz, at T = 30 °C … 90 °C. After each measurement, the sample was depolarized for at least 6 hours between two Rogowski-type electrodes (connected to the ground).

6.2.7. Space charge

The volume charge density for flat samples was determined using the PEA method, described in Chapter 5. For cylindrical samples a similar setup is used, using the same principles but adapted to a cylindrical geometry, where the high voltage and ground electrodes are, here, connected to the inside and outside of the cylindrical samples and the voltage pulses are applied by a pulse generator that is connected to the outside of the sample [268]. In cylindrical sample measurements, the space charge distribution is determined in an area that depends on the length of the piezoelectric sensor and the contact surface between the outside of the sample and the top of the measuring cell.

The equipment used for PEA measurements on flat samples (without adhering electrode materials) and on cylindrical samples is provided by TechIMP (AltaNova) and was present at LIT, Bologna. The measurement sensitivity (on flat and cylindrical samples) is +/- 0.15 C/m^3.

Fig. 10. Electrical conductivity measuring cell

The measurements for flat samples were performed under the following conditions:

- Measurement temperature: 30 °C and 60 °C
- DC voltage, positive polarity, Applied electric field: 1 – 50 kV/mm
- Measurement duration: 1 hour Voltage-ON and 1 hour Voltage-OFF

The measurements for cylindrical samples were performed under following conditions:

- Measurement temperature: 30 °C
- DC voltage, positive polarity: 25, 35, 50, 75 and 100 kV
- Average applied electric field: ≈ 5 – 20 kV/mm
- Measurement duration: 1 hour Voltage-ON and 1 hour Voltage-OFF

The space charge measurement steps (for both flat and cylindrical samples) are presented in section §6.7.3. Of note in this summary are parts of Step 3 (Electrical signal acquisition) and Step 4 (Electrical signal processing), respectively:

- For Voltage-ON measurements on flat samples, the voltage increase to the value established for each measurement was performed continuously, with a slope of approximately 3 kV/s, and for samples with a cylindrical geometry it was continuously increased in 2 s for voltage of 25 kV, 5 s for 50 kV, 10 s for 75 kV and 30 s for 100 kV.
- For Voltage-OFF measurements for flat samples, the voltage was removed by rapidly decreasing its value (in 1 – 2 seconds) to zero, turning off the power supply and connecting both electrodes of the measurement cell to the ground. For samples with cylindrical geometry, the voltage was removed by rapidly decreasing its value (with a slope of approx. 15 kV/s), turning off the power supply and connecting to the ground.
- All the individual electrical signals were processed according to the steps described in §5.2. For the deconvolution stage, the order of the Gaussian filter was 5 and the attenuation and dispersion of the electrical signal were neglected.
- Because the attenuation and dispersion of the electrical signal has been neglected, the correctness of the space charge density distribution obtained from the processing of the electrical signal is verified by an "*additional step*" introduced in the numerical processing stage of the electrical signal from the MATLAB software application. This "*additional step*" consists in determining the distribution of the electric field $E(x)$ (knowing the distribution of the space charge density $\rho_v(x)$), followed by determining the distribution of the electric potential $V(x)$ and checking the boundary conditions (the value of the electric potential at the positions of the two electrodes, x_0 and x_g). If the conditions on the borders are not verified, then the real values are imposed on them and the distribution of the electric field and the space charge density is recalculated.
- The space charge density distribution was determined, for each acquisition, from the measured values of the PEA signal at that moment by a procedure to more correctly describe the charge distribution at a given time, taking into account the transient fluctuations of the signal. The procedure is described in more detail in §6.2.7.3. – Step 4.

The conclusions of Chapter 6 are:

- Flat samples (XLPE, EPR, EPDM, XLPE / EPR, XLPE / EPDM) and cylindrical samples (EPR / XLPE) were carefully manufactured and the flat samples were investigated via optical and scanning electron microscopy (in order to investigate Hypothesis H4 regarding improved insulation manufacturing quality). The multi-layered samples were found to be in good agreement with cable joint insulation design structures used in the literature, and follow the insulation of extruded insulation cables connected with premoulded prefabricated cable joints with elastomeric compounds (presented in-depth in Chapter 2).
- In order to investigate Hypotheses H1 and H2 regarding the negative long-term effects of thermal ageing, the samples were thermally aged for a duration of 30, 60 and 90 days, and their ageing state was ascertained by FTIR measurements.
- The electrical conductivity, electrical permittivity and space charge density were determined, both for the unaged state and for different states of ageing, from measurements performed under different electrical and thermal stresses. For the space charge density and the resulting electrical field, the input electrical signal was processed using a program offered by TechIMP (AltaNova), which has been considerably improved.

Chapter 7. Experimental results

In Chapter 7 are presented the experimental results regarding accelerated thermal ageing of the samples, the shape of the interface for the layered samples (obtained by microscopy) and the influence of working parameters (electrical voltage during the measurement, temperature applied during the measurement and ageing time) on the properties of studied materials: electrical conductivity, electrical permittivity and density of space charge.

7.1. OM and SEM

The surfaces of the uni-layer XLPE and EPR unaged samples are relatively smooth, with no open pores, craters etc. As a result, the multi-layered samples have reduced thicknesses for the intermediate (air) layers (fig. 11). For a more in-depth analysis of the quality of the interfaces, the XLPE / EPR unaged samples were studied via SEM. Some of the results are presented in figs. 12 – 13. Figure 13 shows that there is a continuous area between the two constituent materials, different from the adjacent areas, and that it is about 0.5 micrometers thick in the case of unaged samples.

7.2. DSC and FTIR

DSC measurements were performed in order to determine the maximum permissible ageing temperature of the samples. The results are presented in fig. 14. Based on the melting temperature values for XLPE samples (fig. 14, curve **1**, respectively, 123 °C) and for EPDM samples (fig. 14, curve **2**, respectively, 139 °C), the ageing temperature $T = 120$ °C was selected.

Ageing was performed according to section §6.2.2 at the temperature of 120 °C for three durations, respectively for 30 (I1), 60 (I2) and 90 (I3) days. It was found that, during the ageing processes, the samples undergo a series of physical transformations, respectively visual changes (change of colour to brown) of the samples, both flat and cylindrical, as well as bending deformation of the samples.

The FTIR spectra on the samples show that they underwent thermal ageing differently and are distinct for each ageing state. The presence of different ageing residuals show that the morphological and chemical structure of the samples has changed with the ageing duration, and, thus, it is expected that thermal ageing has an effect on the long term electrical properties and space charge distribution of cable joint insulations (following Hypotheses H1 and H2). Some of the results are shown in fig. 15.

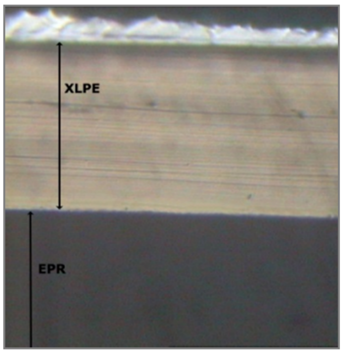

Fig. 11. Interface of the XLPE / EPR unaged samples (OM, 40 X magnification)

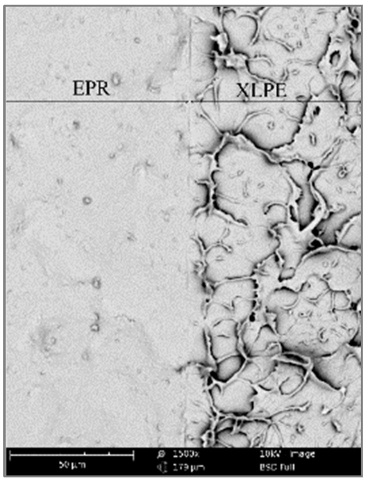

Fig. 12. Interface of the XLPE / EPR unaged samples (SEM, 1500 X magnification)

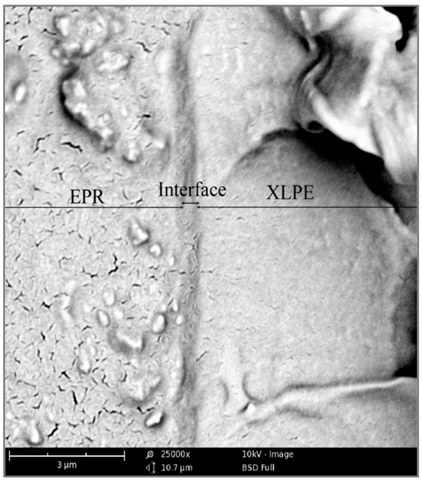

Fig. 13. Interface of the XLPE / EPR unaged samples (SEM, 25000 X magnification)

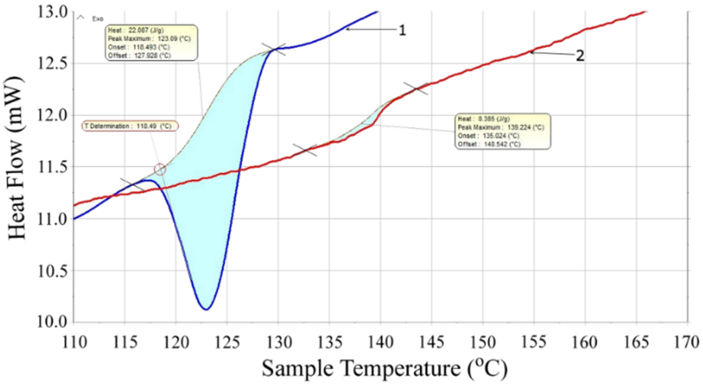

Fig. 14. Determination of melting temperatures for XLPE (1) and EPDM (2) via DSC

The FTIR spectra for XLPE samples, unaged (curve **1**) and aged at 120 °C for 30 (**2**), 60 (**3**) and 90 (**4**) days are presented in fig. 15, *a*. It is found that the thermal stress of XLPE induces in the FTIR spectrum an increase in intensity of the maximum at approx. 1724 cm^{-1} (fig. 15, *a*) due to the formation of carbonyl (-C=O) aldehyde groups [272]. It is also observed an increase of absorbances at approx. 1265 cm^{-1}, respectively at approx. 1095 cm^{-1} due to stretching vibrations of chemical bonds and due to the presence of antioxidants [273].

The FTIR spectra for EPR samples, unaged (curve **1**) and aged at 120 °C for 30 (**2**), 60 (**3**) and 90 (**4**) days are presented in fig. 15, *b*. It is possible to observe an enlargement of the peak included in the region at 1400 – 1800 cm^{-1} (fig. 15, *b*) with the increase of the ageing time, spectral region corresponding to different carbonyl type oxidation compounds (-C=O). This is also correlated with the increase in intensity of the peak of approx. 1320 cm^{-1} due to the stretching vibration of some C-H chemical bonds. The increase in the intensity of these bands is due to the increase in the degree of ageing induced by the heat treatment. The existence of a band with a maximum of approx. 1542 cm^{-1} can be observed in the initial EPR spectrum (fig. 15, *b*, curve **1**), which is not characteristic of this type of material. It is also observed that this band disappears upon thermal exposure of the sample for up to 30 days at 120 °C. This band may come from certain residual compounds in the sample manufacturing process.

Figure 15, *c*, show the spectra for EPDM samples, unaged (curve **1**) and aged at 120 °C for 30 (**2**), 60 (**3**) and 90 (**4**) days. An enlargement of the peak included in the region of 1545 – 1800 cm^{-1} can be observed (fig. 15, ***c***) with the increase of the ageing time, spectral region corresponding to different carbonyl type oxidation compounds (-C=O). This is also correlated with the increase of absorbance in the region of hydroxyl groups (-OH) at approx. 3400 cm^{-1} (fig. 15, ***c***) and with the increase in intensity of the peak from approx. 1320 cm^{-1} due to the stretching vibration of some C-H chemical bonds. The increase in the intensity of these bands is due to the increase in the degree of ageing induced by the heat treatment, an aspect confirmed by other similar results obtained for EPDM samples in the literature [274]. On the other hand, in the spectrum of unaged EPDM samples, it is observed the existence of a band with a max at approx. 1542 cm^{-1} (similar to EPR) which is not characteristic of this type of material. This band disappears upon thermal exposure of the sample for up to 30 days at 120 °C.

7.3. Electrical conductivity

The results of electrical conductivity measurements are presented in figs. 16 – 18.

The electrical conductivity values are decreasing with the measurement time, for all the types of samples, faster in the first seconds and stabilizes after one hour for XLPE samples and more than an hour for EPR or EPDM samples.

The variations of the electrical conductivity with the measurement time for different values of the applied electric field (between 1 and 20 kV/mm) are presented in fig. 16. It is found that for all the samples the electrical conductivity increases with the applied electric field, but more intense for EPR samples (fig. 16, curve **2**) compared to XLPE samples (fig. 16, curve **1**).

The variations of the electrical conductivity with the measurement temperature (for 30 (**1**), 50 (**2**) and 70 °C (**3**)) are presented in fig. 17, *a*, for XLPE and fig. 17, *b*, for EPR. It is found that for all the samples the electrical conductivity increases with the measured temperature, regardless of the value of the applied electric field.

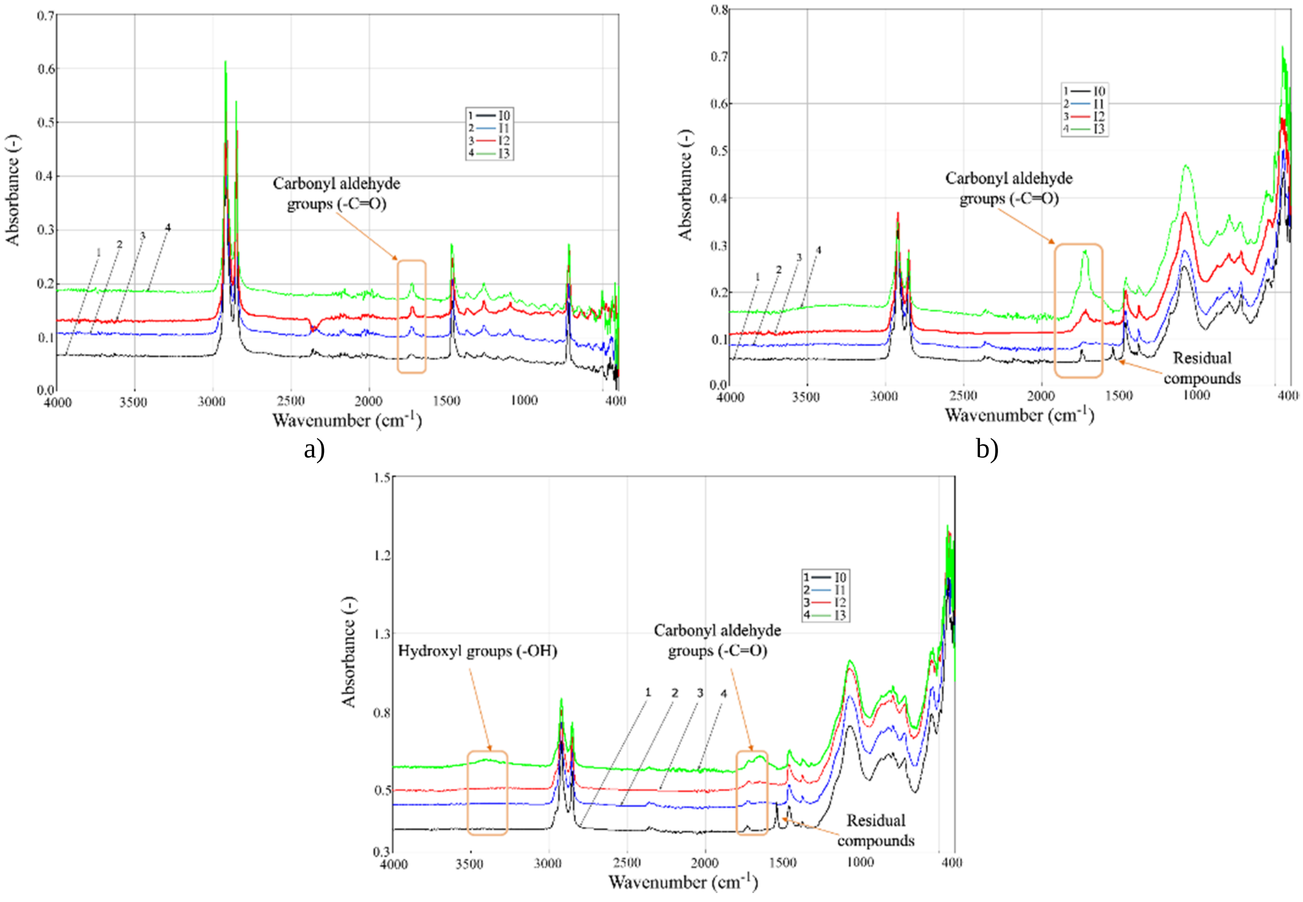

a)

b)

c)

Fig. 15. FTIR spectra for a) XLPE, b) EPR and c) EPDM samples, unaged (**1**) and aged for 30 days (**2**), 60 days (**3**) and 90 days (**4**)

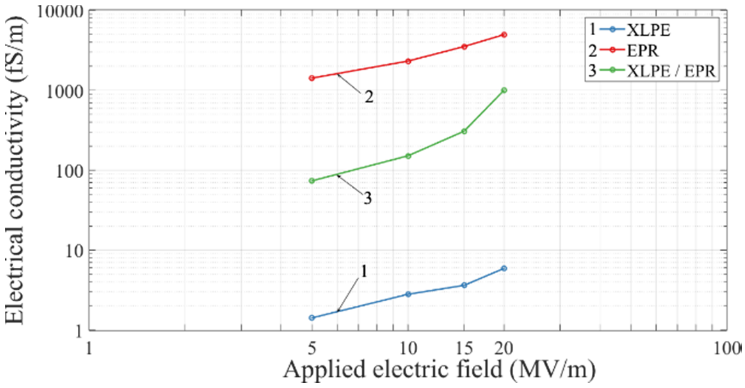

Fig. 16. Variation of the electrical conductivity with the applied electric field, for XLPE (**1**), EPR (**2**) and XLPE / EPR (**3**) unaged samples (t = 3600 s, T = 70 °C)

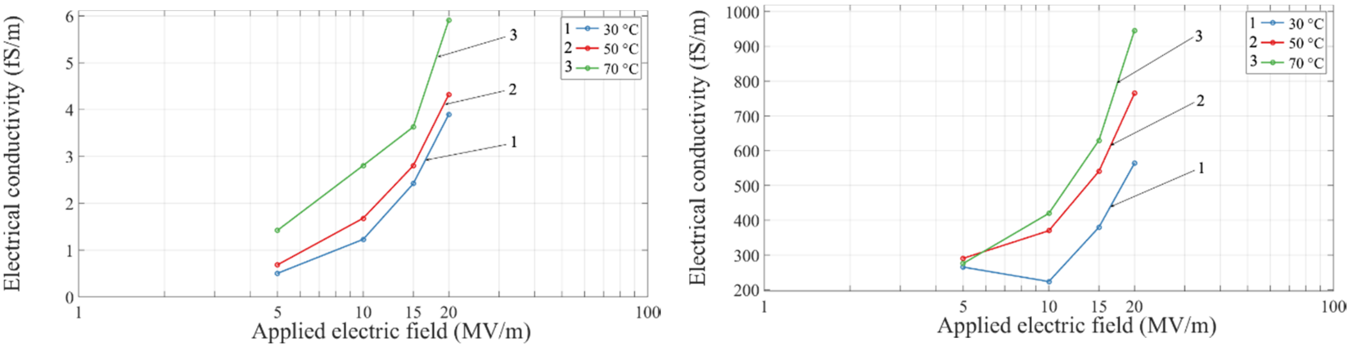

a) b)

Fig. 17. Variation of the electrical conductivity with the applied electric field, for XLPE (a) and EPR (b) unaged samples, at a measurement temperature T = 30 °C (**1**), 50 °C (**2**) and 70 °C (**3**) (t = 3600 s)

Figure 18 shows the variation of the electrical conductivity with the measurement time for unaged (I0) and aged for 30 days (I1), 60 days (I2) and 90 days (I3) flat samples of XLPE (fig. 18, curve **1**), EPR (fig. 18, curve **2**), XLPE / EPR (fig. 18, curve **3**). For all the samples the values of electrical conductivity are higher with thermal ageing, more for EPR or EPDM samples (fig. 18, curve **2**) and less for XLPE samples (fig. 18, curve **1**). Thus, thermal ageing duration has a negative effect on the long term electrical conductivity values of the studied samples (confirming in part Hypothesis H1).

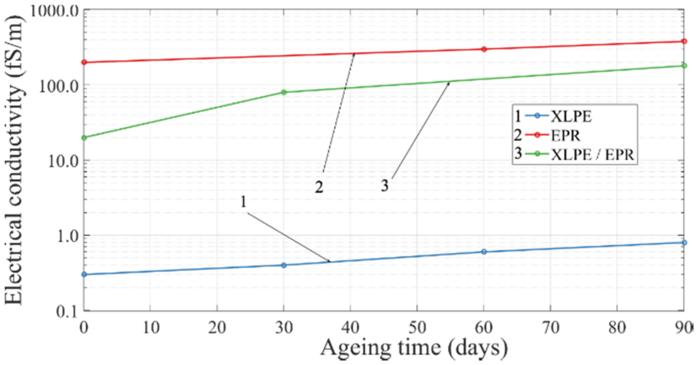

Fig. 18. Variation of the electrical conductivity with the ageing time, for XLPE (**1**), EPR (**2**) and XLPE / EPR (**3**) samples (E_{app} = 1 kV/mm, t = 3600 s, T = 30 °C)

7.4. Electrical permittivity

Using the dielectric spectroscopy method in the frequency range $f = 10^{-2} – 10^{6}$ Hz the real part of the complex electrical permittivity was determined ($\varepsilon_r' = \varepsilon_r$).

A possible link between the variation of the relative permittivity values at low frequencies (close to DC) and the accumulation of space charge (in DC) was not analysed in the thesis, although it is an interesting perspective to pursue for a future study.

Hypothesis H1 which is related to the thermal ageing duration long term effects on the electrical properties (here, electrical permittivity) of cable joint insulations was investigated.

It was found that the values of ε_r increase as the frequency decreases, for all the samples, regardless of their condition (unaged or thermally aged). This is in agreement with other papers [275] and can be explained by the intensification of the local interfacial polarization, by the low-frequency dispersion and by the coupling between negative and positive ions and the formation of new dipoles with enhanced inertia (requiring low frequencies to follow the field).

The variation of ε_r (f = 50 Hz) with the measurement temperature (in °C), for XLPE, EPR and EPDM unaged samples is presented in Table 1. It can be seen that, for all the samples, ε_r decreases with measurement temperature increase. These results are similar to those obtained in the literature for these types of materials [281]. Due to the presence of impurities in the amorphous regions of the sample, all studied materials possess a degree of orientational polarization; thus, the results are attributed, on one hand, to the effect of heat on lowering the orientational polarization due to increased random thermal motion, and on the other hand, to the decrease of the polymer density with the increase of temperature (as the dielectric polarization is reduced due to the lowering of the average number of dipoles per unit volume).

Figure 19 shows the variation of ε_r with the ageing time for the XLPE, EPR and EPDM samples. It is found that this increase in the thermal ageing time determines a reduction of ε_r for the XLPE and EPDM samples and an increase for the EPR samples, results similar to those obtained in the literature for these types of materials ([246], [278], [280]).

Hypothesis H1 is in part confirmed, but only for EPR samples, since for EPDM samples the sum of all the mechanisms involved lowered the relative permittivity values. However, the results do support Hypothesis H4 regarding improved insulation manufacturing quality, since EPR was shown to have a higher ε_r with increased ageing duration (which is due to the presence of more residual products, as previously seen in Chapters 3 and 5).

Table 1. Variation of the relative permittivity (at f = 50 Hz) with the measurement temperature (in °C), for XLPE, EPR and EPDM unaged samples

Material	**Measurement temperature**						
	30 °C	40 °C	50 °C	60 °C	70 °C	80 °C	90 °C
XLPE	2.26	2.20	2.18	2.17	2.16	2.10	2.05
EPR	2.80	2.76	2.74	2.72	2.70	2.66	2.65
EPDM	3.20	3.16	3.13	3.11	3.09	3.08	3.05

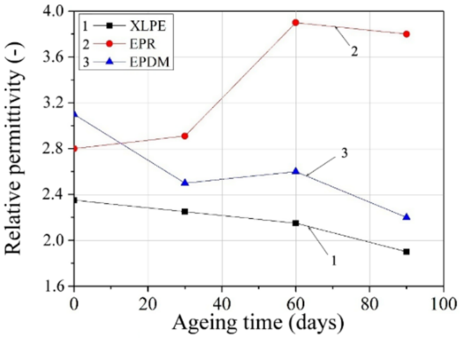

Fig. 19. Variation of the relative permittivity with the ageing time, for XLPE (**1**), EPR (**2**) and EPDM (**3**) (f = 50 Hz, T = 30 °C)

7.5. Space charge

The results of space charge measurements are presented separately for each type of sample and are divided in 4 – 5 categories: variation in time and space, influence of the applied electric field, the influence of the ageing time, the average charge density values, and, for multi-layered samples, the influence of the sample side connected to the High Voltage (HV) electrode.

7.5.1. XLPE (Flat uni-layered samples)

Figure 20 shows the variation of the space charge density ρ_v in time and space for XLPE unaged samples, for E_{app} = 10 kV/mm (for 3600 s during Voltage-ON) and after removing the applied voltage (from 3600 until 7200 s, respectively during Voltage-OFF), with the sample connected between the high voltage electrode (HV) (positive polarity) and the ground electrode (GND). The measuring equipment is connected at GND. Homocharges accumulate near both electrodes during voltage application, and no notable ρ_v accumulates in the bulk of the sample. After removing the voltage, homocharges accumulate near the HV electrode and heterocharges near GND, while in the bulk of the sample a low, positive polarity, ρ_v accumulates.

The ρ_v distribution is also modified by the value of E_{app}, both during Voltage-ON and after removing the applied voltage. In the presence of applied voltage, the increase of E_{app} (from 2 to 30 kV/mm) leads to the increase of ρ_v in the vicinity of the electrodes: of approx. 19 times in the vicinity of the HV electrode and approx. 17 times in the vicinity of GND (fig. 21), and can be attributed to the intensification of the charge injection phenomena at the electrodes.

For all E_{app}, at the points in the vicinity of the ground electrode, ρ_v increases in the first 30 s after voltage application. After 30 s, ρ_v remains constant for E_{app} = 2 – 10 kV/mm and increases for $E_{app} > 10$ kV/mm. In the bulk of the sample, ρ_v increases over time. After removing the voltage, both near the electrodes and in the bulk (middle) of the sample, ρ_v decreases rapidly to a constant (nonzero) value for $E_{app} > 5$ kV/mm and equal to zero for E_{app} = 2 – 5 kV/mm.

The distribution of ρ_v also depends on the ageing time for the XLPE samples, with more changes as the ageing times are longer (fig. 22). It is found that the values of ρ_v are higher in the case of the ageing time of 30 days compared to the duration of 60 days. This could probably be due to the elimination of existing space charge carriers during the thermal stress. As the ageing time increases to more than 60 days, XLPE degrades further, new space charge carriers appear and the values of ρ_v increase. After removing the voltage (Voltage-OFF), in aged samples, ρ_v values decrease in the vicinity of the electrodes and increase in their central areas.

Based on the variations with the coordinate x of ρ_v determined after removing the voltage (at 10 s), the average value of the residual charge density, $\rho_{v,avg}$ was determined for different values of E_{app}. The variations of $\rho_{v,avg}$ with E_{app} and with the ageing time for XLPE samples are presented in fig. 23. $\rho_{v,avg}$ increases with E_{app}, more intense for $E_{app} > 15$ kV/mm for unaged samples and for $E_{app} > 10$ kV/mm for aged samples (threshold corresponding to the intensifications of charge injection mechanisms, which decreases with increasing ageing time), and decrease at the beginning of the thermal stress (first 60 ageing days, fig. 23), but after 90 days they exceed the values of $\rho_{v,avg}$ of unaged samples (point P_3, fig. 23).

7.5.2. EPR (Flat uni-layered samples)

Figure 24 shows the variation of the space charge density ρ_v in time and space for EPR unaged samples, for E_{app} = 10 kV/mm (for 3600 s during Voltage-ON) and after removing the applied voltage (from 3600 until 7200 s, respectively during Voltage-OFF), with the sample connected between the high voltage electrode (HV) of positive polarity and the ground electrode (GND). The measuring equipment is connected to GND. It is found that, during the application of the voltage, charges of positive polarity accumulate near the ground electrode and move in time towards the bulk of the sample. After removing the voltage, the accumulated charges move toward the ground electrode and disappear in approx. 20 minutes.

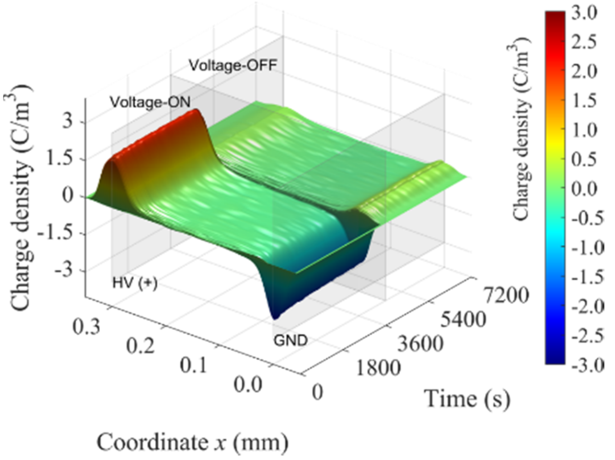

Fig. 20. Variation of the space charge density with the measurement time and with the coordinate *x*, for XLPE unaged samples (E_{app} = 10 kV/mm)

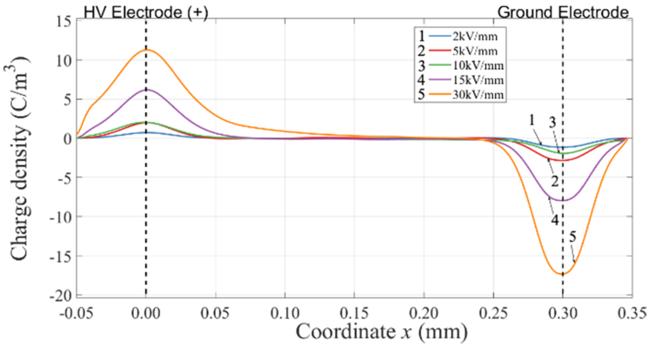

Fig. 21. Variation of the space charge density with the coordinate *x*, at an hour after voltage application, for XLPE unaged samples at E_{app} = 2 (**1**), 5 (**2**), 10 (**3**), 15 (**4**) and 30 (**5**) kV/mm (t = 3600 s, Voltage-ON)

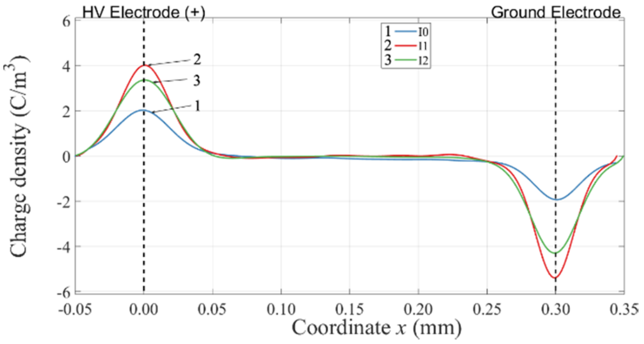

Fig. 22. Variation of the space charge density with the coordinate *x*, at an hour after voltage application, for unaged (I0, **1**) and aged for 30 days (I1, **2**) and 60 days (I2, **3**) XLPE samples (t = 3600 s, E_{app} = 10 kV/mm, Voltage-ON)

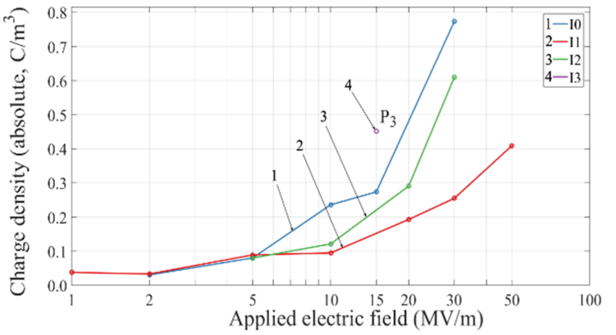

Fig. 23. Variation of the average charge density with the applied electric field, for unaged (I0, **1**), aged for 30 days (I1, **2**), 60 days (I2, **3**) and 90 days (I3, **4**, point P_3) XLPE samples, at 10 s after removing the voltage

The ρ_v distribution is also modified by the value of E_{app}, both during Voltage-ON and Voltage-OFF. In Voltage-ON, the increase of E_{app} (from 2 to 30 kV/mm) leads to the increase of ρ_v in the vicinity of the electrodes: of approx. 4 times in the vicinity of the HV electrode and approx. 5 times in the vicinity of GND (fig. 25). This is due to the intensification of the charge injection phenomena at the electrodes [294]. The space charge packet present in the bulk of the sample changes its position and amplitude with the increase of E_{app} : at the same instant (3600 s) its amplitude is higher, it is wider in space and it is closer to the HV electrode.

For all the values of E_{app}, at the points in the vicinity of the ground electrode (at x_P = 0.47 mm), ρ_v increases in the first 5 minutes after the application of the voltage, and after that ρ_v remains constant for E_{app} = 2 – 15 kV/mm and decreases for E_{app} > 15 kV/mm. In the bulk of the sample ρ_v values increase over time, but are affected by the moving charge packet. After removing the voltage, ρ_v distribution changes. The maximum values of ρ_v, located in the vicinity of the electrodes, move towards the interior of the samples, and the amplitude of the charge packet in the bulk of the sample decreases, faster for higher values of E_{app} and slower for lower values of E_{app}. After 20 minutes, the values of ρ_v near the ground electrode remain constant, equal to zero for E_{app} < 20 kV/mm and non-zero for higher values of E_{app}, and in the bulk of the sample it remains at a value different than zero for any value of E_{app}.

The distribution of the space charge density also depends considerably on the ageing time for the EPR samples. During Voltage-ON, the values of ρ_v in the vicinity of GND decrease in the aged samples compared to the unaged samples, especially as the ageing times are longer (fig. 26), which shows that space charge with polarity contrary to the GND electrode polarity accumulates in its vicinity, as highlighted by other authors for aged EPR samples [246].

The values of ρ_v corresponding to the space charge packet present in the bulk of the sample are lower, but that they are closer to the HV electrode with the longer ageing times. This is probably due to the change in the chemical structure of the EPR, on one hand due to the increase in the number of deep traps in which the space charge carriers are trapped (decreasing the maximum value of the space charge packet with the ageing time) [246], and on the other hand due to facilitating the phenomenon of diffusion of space charge carriers in the sample (by increasing the mobility of the space charge packet) when moving in the bulk of the sample.

During Voltage-ON, near GND, the values of ρ_v increase (faster) in the first 10 minutes and then decrease in time, at values depending on the ageing time (highest for the unaged sample and lowest for the 60 days aged). After Voltage-OFF it is observed that charge of polarity opposite to that of the electrode accumulates near the ground electrode (heterocharge), at a higher amplitude for aged samples, and that for aged samples there is a negative polarity charge in the central sample area. The variation of the space charge density with the measurement time is similar to that in the case of applied voltage, with values of ρ_v decreasing faster the more aged the sample is, becoming positive (homocharge becomes heterocharge in time) and stabilizing at values higher than those of unaged samples.

The values of $\rho_{v,avg}$ increase with E_{app} and the threshold of charge injection is lower in the case of aged than of unaged samples (E_{app} > 10 kV/mm, unaged, and E_{app} > 5 kV/mm, aged samples). $\rho_{v,avg}$ decreases at the beginning of the thermal stress (first 60 ageing days, fig. 27), but after 90 days they exceed the values of $\rho_{v,avg}$ of unaged samples (point P_3 of fig. 27).

7.5.3. EPDM (Flat uni-layered samples)

Figure 28 shows the variation of the space charge density ρ_v in time and space for EPDM unaged samples, for E_{app} = 10 kV/mm (for 3600 s during Voltage-ON) and after removing the applied voltage (from 3600 until 7200 s, respectively during Voltage-OFF), with the sample connected between the HV electrode of positive polarity and GND. The measuring equipment is connected to GND. During the application of the voltage, homocharge accumulates in time near the HV electrode and charges of negative polarity accumulate near the ground electrode and move in time towards the bulk of the sample, leaving at the position of the ground electrode a charge of positive polarity. After removing the voltage, a large portion of the positive and negative charges in the bulk of the sample towards the ground electrode are recombined and disappear, in contrast to the charges in the vicinity of the ground electrode (of positive polarity, heterocharge) that remain near the electrode until the end of the measurement.

The ρ_v distribution is also modified by the value of E_{app}, both during Voltage-ON and during Voltage-OFF. In the presence of applied voltage (fig. 29), the increase of E_{app} (from 2 to 30 kV/mm) leads to an injection of space charge from the HV electrode in its vicinity (homocharge) and, for E_{app} > 10 kV/mm, injection of space charge of positive polarity near the GND electrode (heterocharge). The space charge packet found in the bulk of the sample increases in amplitude but does not change its position (compared to EPR, see fig. 25).

Results reported in the literature for EPDM differ depending on the type of diene used in the sample manufacturing process (some accumulate homocharge, others heterocharge [62]), but, in general, they present homocharge injection from both electrodes for E_{app} > 10 kV/mm, and, for E_{app} > 20 kV/mm an accumulation of heterocharge near the HV electrode [295]. The results obtained here show a similar behaviour, with the accumulation of heterocharge appearing, in this case, also at values of E_{app} > 20 kV/mm, but near the ground electrode.

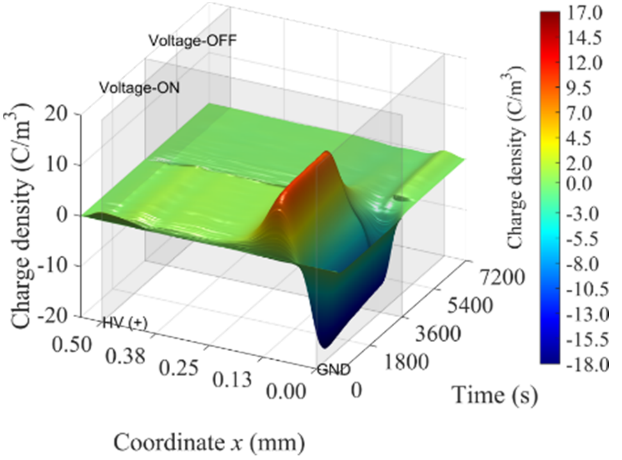

Fig. 24. Variation of the space charge density with the measurement time and with the coordinate *x*, for EPR unaged samples (E_{app} = 10 kV/mm)

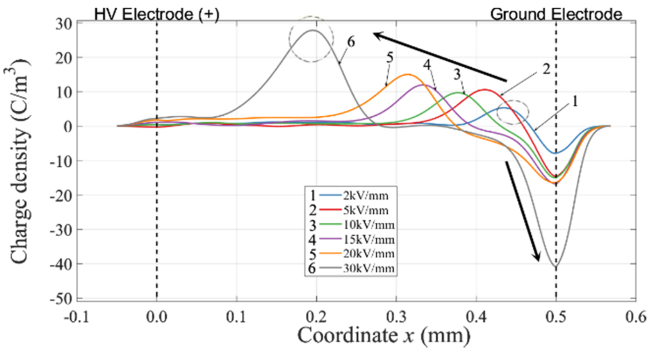

Fig. 25. Variation of the space charge density with the coordinate *x*, at an hour after voltage application, for EPR unaged samples at E_{app} = 2 (1), 5 (2), 10 (3), 15 (4) and 30 (5) kV/mm (t = 3600 s, Voltage-ON)

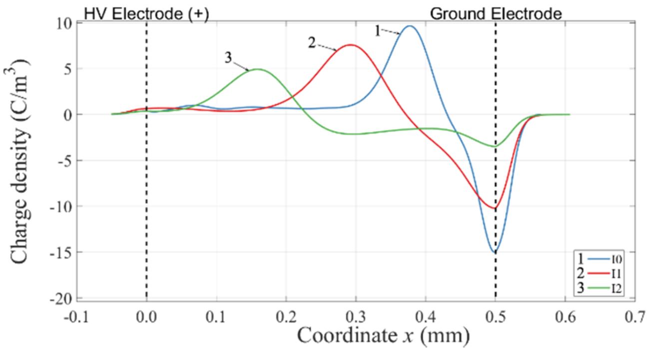

Fig. 26. Variation of the space charge density with the coordinate *x*, at an hour after voltage application, for unaged (I0, 1) and aged for 30 days (I1, 2) and 60 days (I2, 3) EPR samples (t = 3600 s, E_{app} = 10 kV/mm, Voltage-ON)

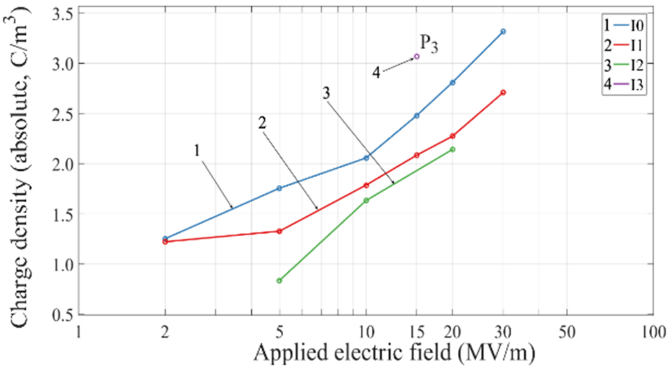

Fig. 27. Variation of the average charge density with the applied electric field, for unaged (I0, 1), aged for 30 days (I1, 2), 60 days (I2, 3) and 90 days (I3, 4, point P_3) EPR samples, at 10 s after removing the voltage

For all the values of E_{app}, at the points in the vicinity of the HV electrode (at x_P = 0.02 mm), ρ_v increases rapidly in the first seconds after the application of the voltage, and after that ρ_v continues to increase (proportional to the value of E_{app}). In the bulk of the sample the values of the space charge density decrease over time. The following is observed after removing the voltage: homocharge near HV, heterocharge near GND and a negative polarity space charge density in the bulk of the sample around the position x_P = 0.42 mm. Over time, both near the electrodes and in the bulk of the sample, ρ_v decreases to values close to zero.

The distribution of ρ_v also depends considerably on the ageing time for the EPDM samples. During Voltage–ON it is observed the presence of a charge density of positive polarity in the bulk of the sample in the case of aged samples compared to the unaged samples and also that the values of ρ_v corresponding to the space charge packet present in the sample are higher (fig. 30). This phenomenon is more than likely due to the thermo-oxidative effects due to the ageing of the samples, the consumption of antioxidants or their poor efficiency in the case of an amorphous material such as EPDM [174], the breaking of chemical bonds of EPDM and the increase of the number of space charge carriers (polar groups, ionic species) [295].

After Voltage-OFF, charge of polarity opposite to that of the electrode accumulates near GND (heterocharge) with a higher amplitude for aged samples, and for aged samples there are space charges of both polarities in the central sample area (of positive polarity towards the HV electrode and of negative polarity towards GND). Over time, ρ_v near GND decreases in amplitude but does not reach zero values, the values being higher the more the sample is aged.

The variations of $\rho_{v,avg}$ with E_{app} and with the ageing time for EPDM samples are presented in fig. 31. It is found that the values of $\rho_{v,avg}$ increase with E_{app} (more intense for $E_{app} > 5$ kV/mm, the threshold corresponding to the intensifications of charge injection mechanisms, see §4.4), and that the values of $\rho_{v,avg}$ for the aged samples exceed the values of $\rho_{v,avg}$ corresponding to the unaged samples (points P_2 and P_3 compared to point P_1 in fig. 31).

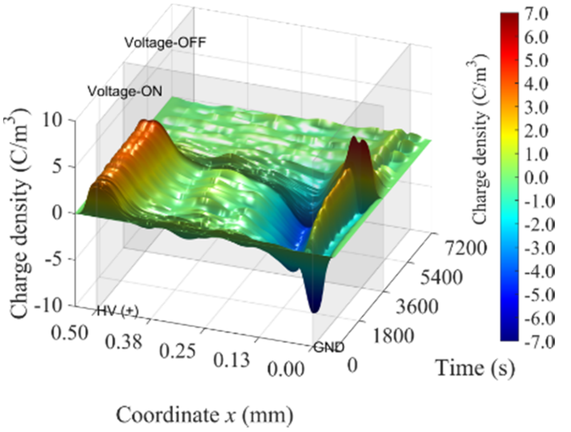

Fig. 28. Variation of the space charge density with the measurement time and with the coordinate *x*, for EPDM unaged samples (E_{app} = 10 kV/mm)

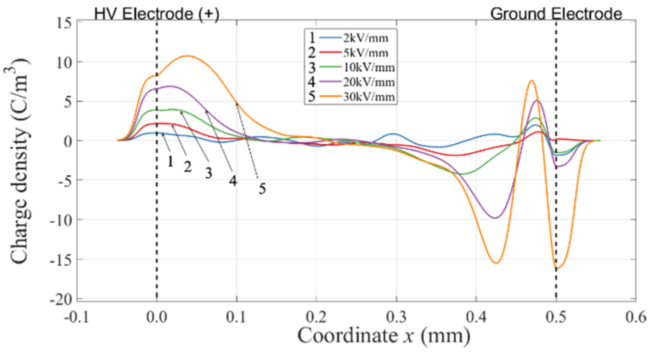

Fig. 29. Variation of the space charge density with the coordinate *x*, at an hour after voltage application, for EPDM unaged samples at E_{app} = 2 (1), 5 (2), 10 (3), 15 (4) and 30 (5) kV/mm (t = 3600 s, Voltage-ON)

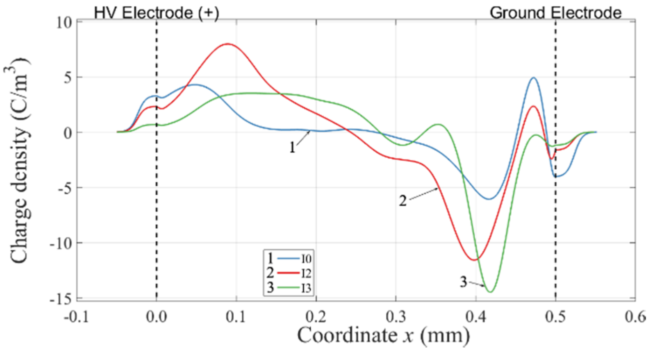

Fig. 30. Variation of the space charge density with the coordinate *x*, at an hour after voltage application, for unaged (I0, 1) and aged for 60 days (I2, 2) and 90 days (I3, 3) EPDM samples (t = 3600 s, E_{app} = 15 kV/mm, Voltage-ON)

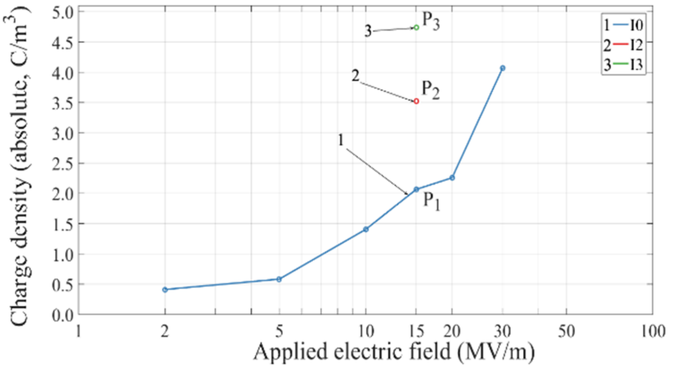

Fig. 31. Variation of the average charge density with the applied electric field, for unaged (I0, 1), aged for 60 days (I2, 2, point P_2) and 90 days (I3, 3, point P_3) EPDM samples, at 10 s after removing the voltage

7.5.4. XLPE / EPR (Flat multi-layered samples)

Figure 32 shows the variation of the space charge density ρ_v in time and space for XLPE / EPR unaged samples, for E_{app} = 10 kV/mm (for 3600 s during Voltage-ON) and after removing the applied voltage (from 3600 until 7200 s, respectively during Voltage-OFF), with the sample connected between the HV electrode of positive polarity and GND, with the XLPE side connected to HV. The measuring equipment is connected to GND. During voltage application, charges of positive polarity accumulate near GND and at the interface of XLPE and EPR; charges of negative polarity accumulate in the bulk of the XLPE layer of the sample. After removing the voltage, the accumulated charges near GND move toward the electrode and their amplitude reduces with the measurement time (but does not become zero), the accumulated charges at the interface of XLPE and EPR change their polarity from negative to positive and remain in the area of the interface and the accumulated charges in the bulk of the XLPE layer of the sample are reduced with the measurement time, but do not become zero.

For the multi-layered XLPE / EPR samples, ρ_s accumulates at the interface. When XLPE is connected to HV, during voltage application, ρ_s accumulates to negative values in the first 3 minutes and, after, its value decreases over time. After removing the voltage, ρ_s changes its polarity (in about 1 minute) and decreases slightly (but does not cancel even after an hour).

The ρ_v distribution is also modified by the value of E_{app}, both during Voltage-ON and Voltage-OFF. In Voltage-ON, the increase of E_{app} (from 5 to 15 kV/mm) leads to the increase of ρ_v, both in the vicinity of the HV electrode, where it increases approx. 6 times, and in the bulk of the sample in the XLPE side of the interface, where it increases approx. 5 times (fig. 33). After removing the voltage, the ρ_v distribution changes: it decreases in the vicinity of the HV electrode and at the interface and increases in the vicinity of GND. These variations are more important in the case of higher values of E_{app}. The ρ_v near GND decreases over time to a constant positive value, faster if the value of E_{app} is higher, and ρ_v at the interface tends to zero for E_{app} = 5 kV/mm and to a constant positive value for higher values of E_{app}.

The value of E_{app} also modifies the surface charge density ρ_s that accumulates at the interface. It is found that ρ_s increases with E_{app} and that, after removing the voltage, ρ_s goes in time to zero for E_{app} = 5 kV/mm and to constant, positive values, for E_{app} > 5 kV/mm (fig. 34).

The distribution of ρ_v also depends on the ageing time for the XLPE / EPR samples; during Voltage–ON in the aged samples the values of ρ_v increase, both in the vicinity of the electrodes and in the bulk of the sample (fig. 35). During Voltage-OFF, in aged samples, the ρ_v values decrease in the vicinity of HV, changes its polarity in the vicinity of GND and increases in the sample's bulk. These variations become more important for longer ageing times.

The sample side connecting to the HV electrode was found to also influence the values of ρ_v. During Voltage-ON, when XLPE is connected to the HV electrode, the ρ_v in the vicinity of both electrodes is of positive polarity (homocharge at the HV electrode and heterocharge at GND) and in the vicinity of the interface is of negative polarity. When EPR is connected to the HV electrode, ρ_v in the vicinity of both electrodes has negative polarity (heterocharge at the HV electrode and homocharge at GND) and in the vicinity of the interface ρ_v is of positive polarity.

The variations of $\rho_{v,avg}$ with E_{app} and with the ageing time for XLPE / EPR samples, with XLPE connected to the HV electrode, are presented in fig. 36. $\rho_{v,avg}$ increases with E_{app} and, for all E_{app}, $\rho_{v,avg}$ corresponding to aged samples are higher than for unaged samples.

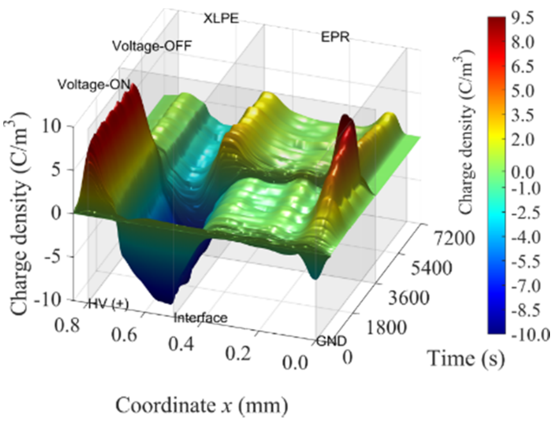

Fig. 32. Variation of the space charge density with the measurement time and with the coordinate *x*, for XLPE / EPR unaged samples (E_{app} = 10 kV/mm)

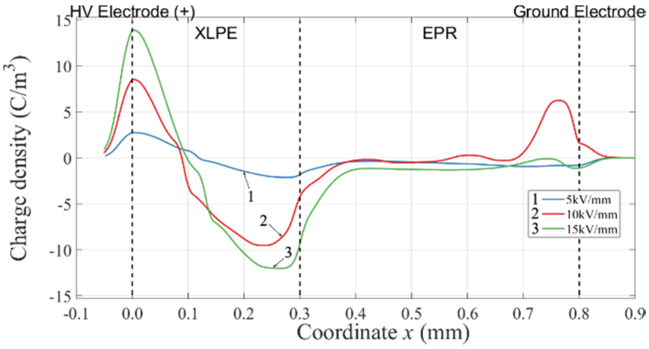

Fig. 33. Variation of the space charge density with the coordinate *x*, at an hour after voltage application, for XLPE / EPR unaged samples at E_{app} = 5 (**1**), 10 (**2**) and 15 (**3**) kV/mm (t = 3600 s, Voltage-ON)

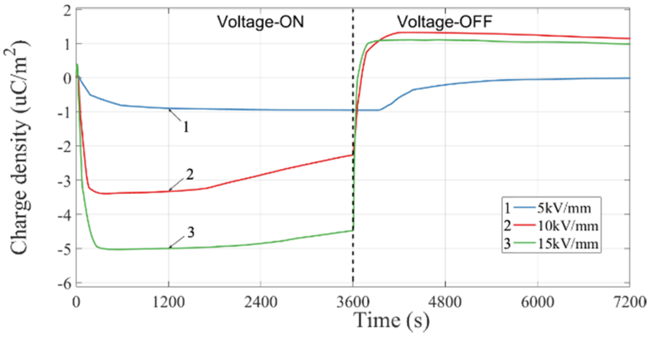

Fig. 34. Variation with the measurement time of the surface charge density at a point $P(x_P)$ on the interface of XLPE / EPR unaged samples, at E_{app} = 5 (**1**), 10 (**2**) and 15 (**3**) kV/mm (x_P = 0.30 mm)

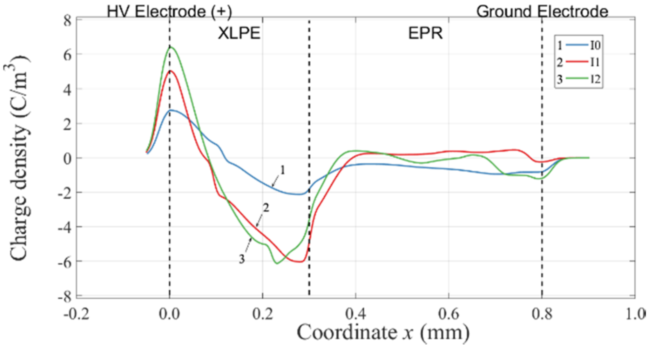

Fig. 35. Variation of the space charge density with the coordinate *x*, at an hour after voltage application, for unaged (I0, **1**) and aged for 30 days (I1, **2**) and 60 days (I2, **3**) XLPE / EPR samples (t = 3600 s, E_{app} = 5 kV/mm, Voltage-ON)

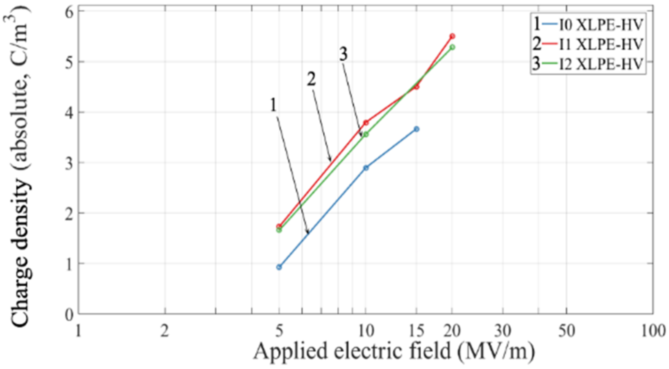

Fig. 36. Variation of the average charge density with the applied electric field, for unaged (I0, **1**), aged for 30 days (I1, **2**) and 60 days (I2, **3**) XLPE / EPR samples, at 10 s after removing the voltage

7.5.5. XLPE / EPDM (Flat multi-layered samples)

Figure 37 shows the variation of the space charge density ρ_v in time and space for XLPE / EPDM unaged samples, for E_{app} = 10 kV/mm (for 3600 s during Voltage-ON) and after removing the applied voltage (from 3600 until 7200 s, respectively during Voltage-OFF), with the sample connected between the HV electrode of positive polarity and GND. The XLPE side of the sample is connected to the HV electrode and the measuring equipment is connected to GND. During the application of the voltage, charges of opposite polarity accumulate in the vicinity of each electrode (heterocharge), a charge of positive polarity accumulates in the bulk of the sample and a charge of negative polarity accumulates at the interface between XLPE and EPDM. When the voltage is removed, the ρ_v accumulated during the application of the voltage disappears quickly.

For the multi-layered XLPE / EPDM samples, the surface charge density ρ_s that accumulates at the interface between the materials when XLPE is connected to the HV electrode was determined and it was found that, during voltage application, ρ_s of negative polarity accumulates in the interface area in the first 8 minutes and, after that, its value remains quasi-constant over time. After removing the voltage, ρ_s decreases, at the beginning very quickly (in approx. 1 min reaching 35% of the initial value) and then, relatively slower, but does not cancel even after one hour.

The ρ_v distribution is also modified by the value of E_{app}, both during Voltage-ON and after removing the applied voltage. In the presence of applied voltage, the increase of E_{app} from 5 to 15 kV/mm leads to the increase of ρ_v values, both in the vicinity of the electrode (in the vicinity of the ground electrode it increases approx. 2.7 times) and in the bulk of the sample (at the interface area between XLPE and EPDM it increases approx. 2 – 3 times) (fig. 38).

After removing the voltage, the space charge density decreases in the whole sample, the decrease is more pronounced in the bulk of the sample than near the electrodes. The space charge density near GND decreases in the first 3 minutes towards zero for $E_{app} < 15$ kV/mm and towards a constant negative value for $E_{app} = 15$ kV/mm. The surface charge density at the interface also decreases over time down to non-zero values, higher for higher values of E_{app}.

The sample side connecting to the HV electrode was found to also influence the values of ρ_v, and in both cases at the interface between XLPE and EPDM a charge of negative polarity accumulates during voltage application, and a charge of positive polarity accumulates after removing the voltage. In both methods of connecting the sample, space charge accumulates near the electrodes, of opposite polarity to the polarity of the electrode (heterocharge). Also, ρ_v is higher near the electrodes in the case where EPDM is connected at the HV electrode.

There are also notable differences in the distribution of ρ_s in the interface area between the two cases. When XLPE is connected to the HV electrode, ρ_s is of negative polarity and increases in the first minutes from voltage application, stabilizing after approx. 3600 s. When the voltage is removed, ρ_s decreases first very quickly and then slowly stabilizes after approx. 3600 s. When EPDM is connected to the HV electrode ρ_s is negative, increases rapidly in the first seconds and then decreases, reaching a positive polarity at 3600 s. After removing the voltage, ρ_s increases rapidly and remains at a quasi-constant, positive value (fig. 39).

The variations of $\rho_{v,avg}$ with E_{app} and with the ageing time for XLPE / EPDM samples are presented in fig. 40. It is found that the values of $\rho_{v,avg}$ increase with E_{app} (faster for $E_{app} > 10$ kV/mm, the threshold corresponding to the intensifications of charge injection mechanisms, see §4.4), and that they are higher for the case of measurements where EPDM was connected to the HV electrode.

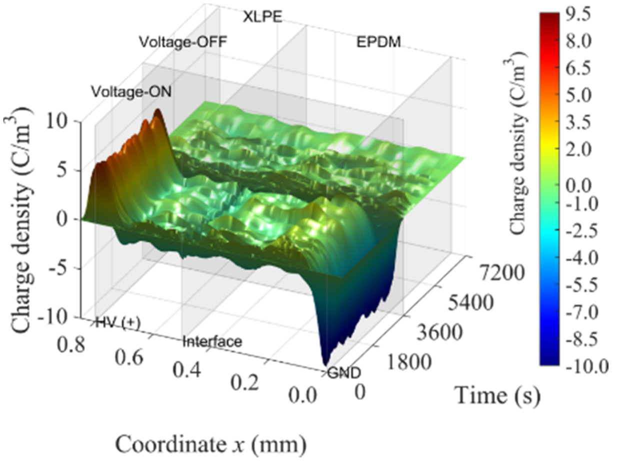

Fig. 37. Variation of the space charge density with the measurement time and with the coordinate *x*, for XLPE / EPDM unaged samples (E_{app} = 10 kV/mm)

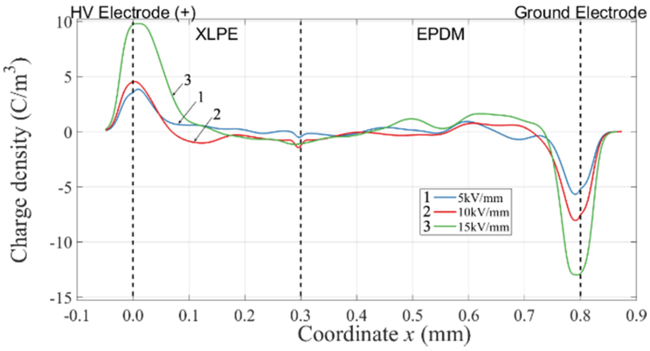

Fig. 38. Variation of the space charge density with the coordinate *x*, at an hour after voltage application, for XLPE / EPDM unaged samples at E_{app} = 5 (1), 10 (2) and 15 (3) kV/mm (t = 3600 s, Voltage-ON)

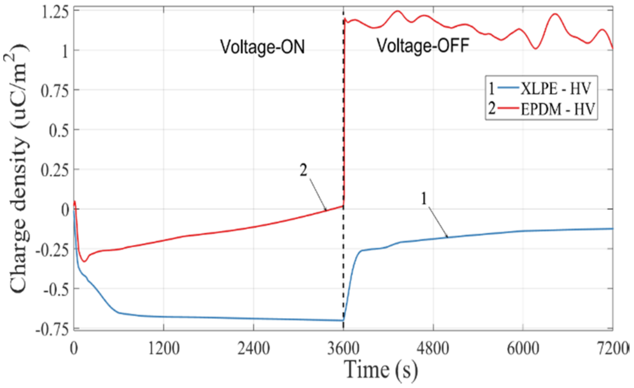

Fig. 39. Variation with the measurement time of the surface charge density at a point $P(x_P)$ on the interface of XLPE / EPDM unaged samples, with XLPE (x_P = 0.30 mm, **1**) and with EPDM (x_P = 0.50 mm, **2**) connected to the HV electrode (E_{app} = 10 kV/mm)

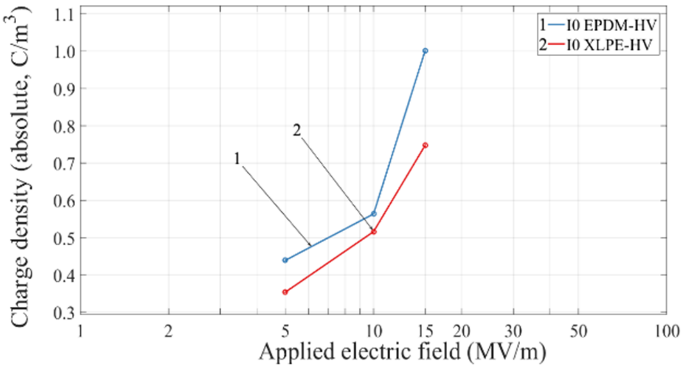

Fig. 40. Variation of the average charge density with the applied electric field, for unaged XLPE / EPDM samples, with XLPE (**1**) and with EPDM (**2**) connected to the HV electrode, at 10 s after removing the voltage

7.5.6. EPR / XLPE (Cylindrical samples)

Figure 41 shows the variation of the space charge density ρ_v in time and space for EPR / XLPE unaged cylindrical samples, for U_{app} = 75 kV (for 3600 s during Voltage-ON) and after removing the applied voltage (from 3600 until 7200 s, respectively during Voltage-OFF), with the sample connected between the HV electrode of positive polarity and GND. The EPR layer is connected to the HV electrode and the measuring equipment is connected to GND. During voltage application, space charge of positive polarity accumulates, both in the bulk of the sample and near the ground electrode, and space charge of negative polarity accumulates at the EPR / XLPE interface area. When removing the voltage, space charge of positive polarity moves from the HV electrode towards the bulk of the sample and space charge of negative polarity accumulates at the EPR / XLPE interface area.

For the multi-layered EPR / XLPE samples, the surface charge density ρ_s that accumulates at the interface between the materials is presented in fig. 42. During voltage application, ρ_s of positive polarity accumulates in the interface area and that, after removing the voltage, ρ_s changes its polarity and increases, at the beginning very quickly (in approx. 1 minute reaching from +2 μC/m^2 to -4 μC/m^2), then, slower (reaching in approx. 8 minutes to -7 μC/m^2), and then, after 12 minutes, starts to slowly decrease (at 3600 s after removing the voltage reaching down to approx. -6 μC/m^2). The existence of ρ_s determines the existence of a residual electric field in the insulation of the cable joints even after their removal from voltage.

The ρ_v distribution is also modified by the value of U_{app}. Increasing the applied voltage from 25 to 100 kV leads to the increase of ρ_v values, both in the vicinity of the electrodes (in the vicinity of the HV electrode up to 4 times and in the vicinity of the ground electrode up to 15 times), as well as in the bulk of the sample (fig. 43).

At the EPR / XLPE interface area, the value of the surface charge density is higher as the value of U_{app} is higher, and increases over time up to 300 s for U_{app} = 25 kV, 1800 s for U_{app} = 50 and 75 kV and 600 s for U_{app} = 100 kV, after which it starts to decrease slowly until the end of the measurement time.

The variations of $\rho_{v,avg}$ with the maximum value of the applied electric field E_{max} (defined in §7.6.1) are presented in fig. 44. It is found that the values of $\rho_{v,avg}$ increase linearly with E_{max} for U_{app} = 25 – 75 kV and that for U_{app} = 100 kV the slope changes, which indicates an intensification of the charge injection mechanisms (see §4.4).

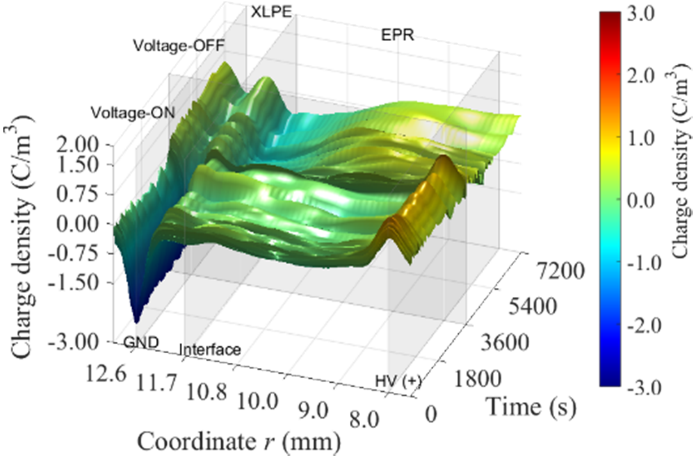

Fig. 41. Variation of the space charge density with the measurement time and with the coordinate r, for EPR / XLPE unaged samples (U_{app} = 75 kV)

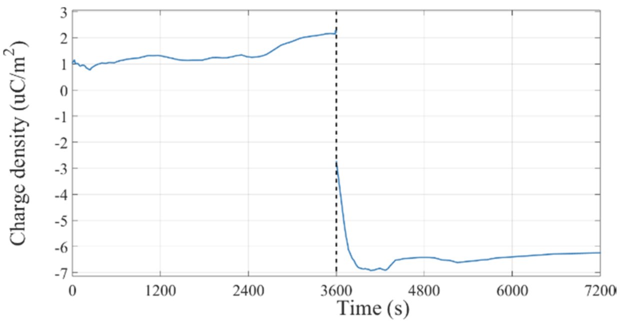

Fig. 42. Variation with the measurement time of the surface charge density at a point $P(r_P)$ on the interface of EPR / XLPE unaged samples (r_P = 11.70 mm, U_{app} = 100 kV)

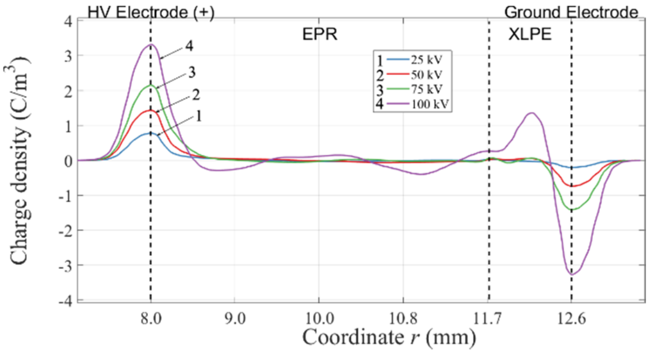

Fig. 43. Variation of the space charge density with the coordinate r, at an hour after voltage application, for EPR / XLPE unaged samples at E_{app} = 25 (**1**), 50 (**2**), 75 (**3**) and 100 (**4**) kV (t = 3600 s, Voltage-ON)

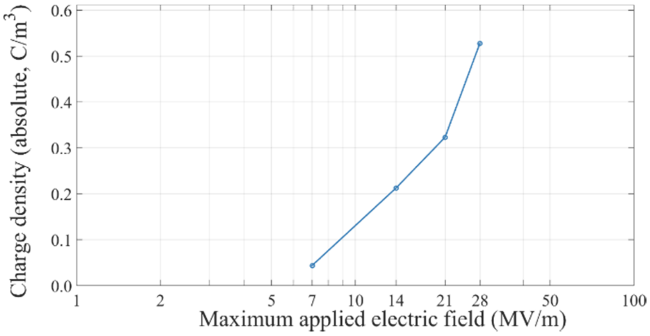

Fig. 44. Variation of the average charge density with the maximum applied electric field, for EPR / XLPE unaged samples, at 10 s after removing the voltage

7.6. Reduction of space charge

In all types of samples (flat and cylindrical) manufactured from XLPE, EPR and EPDM, space charge is present, and, in the case of multi-layered samples a surface charge density is separated at their interfaces. The presence of this space charge leads to the local intensification of the electric field in the samples and to the generation of important residual electric fields. It results that in the insulations of the DC cable joints manufactured from these materials, in operation, these phenomena will take place. Their most important effects will be the accelerated degradation of the insulations, both during operation and after the de-energization of the cable joints (due to residual electric fields). The insulation materials used for the cable joints must have the lowest possible value of space charge accumulated in their operation.

The three materials studied in this chapter exhibit different values of the residual charge density $\rho_{v,avg}$. As shown in fig. 45, for the same value of the applied electric field, below 25 kV/mm, the XLPE samples (fig. 45, curve **1**) present the lowest values of $\rho_{v,avg}$, followed by EPR (fig. 45, curve **2**) and EPDM (fig. 45, curve **3**); for over 25 kV/mm, EPDM samples show the highest values for $\rho_{v,avg}$. Moreover, the threshold corresponding to the intensification of charge injection mechanisms is different; it is approximately 15 kV/mm for XLPE (fig. 45, curve **1**), 10 kV/mm for EPR (fig. 45, curve **2**) and 7 kV/mm for EPDM (fig. 45, curve **3**).

In the multi-layered samples, at the interfaces between the layers, a surface charge density ρ_s is separated, whose values depend on the values of conductivity and permittivity of the two layers and on the interface characteristics. The values of ρ_s are lower in the case of XLPE / EPDM samples (fig. 46, curve **1**) than in the case of XLPE / EPR (fig. 46, curve **2**). The values of ρ_s determined in the vicinity of the interfaces are relatively important and are dependent on the applied electric field at the start of the measurements (fig. 34).

The average charge density $\rho_{v,avg}$ obtained for the unaged flat multi-layered samples depends both on E_{app} and on the characteristics of the samples; its size increases with the value of E_{app} for all samples, higher for XLPE / EPR samples and lower for XLPE / EPDM samples.

Measurements performed on thermally aged samples show that the values of ρ_v have changed, following ageing, in all samples (fig. 47 for E_{app} = 15 kV/mm). As the duration of ageing has been relatively short (90 days), its effects on increasing space charge values are not very spectacular, but a number of other studies show that ρ_v values increase during operation.

There were higher variations of the residual average charge density in the EPR samples (fig. 47, curve **2**) and EPDM samples (fig. 47, curve **3**) and smaller variations in the XLPE samples (fig. 47, curve **1**). The increase of the ageing time determines important increases of the value of $\rho_{v,avg}$ in the EPDM samples (from 2 to 4.75 C/m^3) and decreases, initially, followed by increases, in the case of EPR samples (from 2.5 to 2 C/m^3 in the first 60 days, followed by an increase to 3 C/m^3 in the last 30 days) and, less so in the case of XLPE samples (0.25 to 0.20 C/m^3 in the first 30 days, followed by an increase to 0.50 C/m^3 in the last 60 days).

The average charge density $\rho_{v,avg}$ depends to a large extent on the characteristics of the interface; flat samples manufactured by pressing (fig. 48, curve **1**) show a higher value of $\rho_{v,avg}$ than cylindrical samples manufactured by triple extrusion (fig. 48, curve **2**).

The insulation materials used for the cable joints must have the lowest possible value of space charge accumulated in their operation. The purity of the basic materials and the manufacturing technology must be improved. Materials that have smaller variations of ρ_v and $\rho_{v,avg}$ should be used, respectively between the studied materials, EPDM is preferable.

Because XLPE is currently the basic material for the insulation of DC power cables, the reduction of space charge can be achieved by improving the degree of purity (physical, without contaminants, and chemical, reduced number of additional chemical species that introduce space charge carriers) of the base material, a suitable selection of the introduced additives (invariably introducing more charge carriers) and an increased quality of the technological manufacturing processes (reduction of the technological residue concentrations).

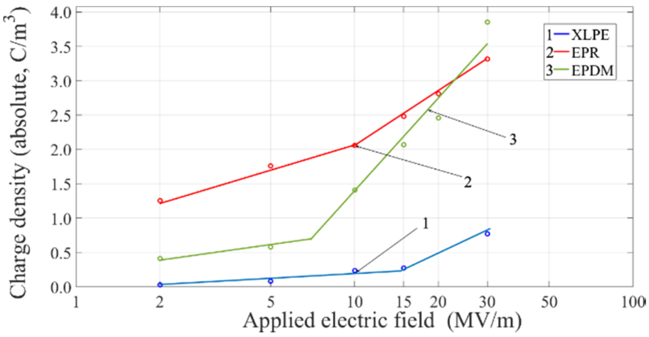

Fig. 45. Variation of the average charge density with the applied electric field,
for XLPE (**1**), EPR (**2**) and EPDM (**3**) unaged samples, at 10 s after removing the voltage

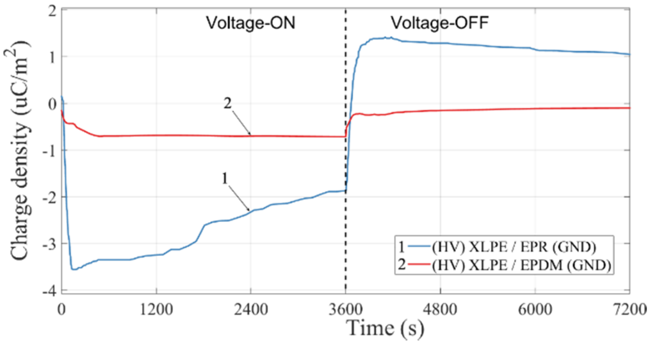

Fig. 46. Variation with the measurement time of the surface charge density at a point $P(x_P)$ on the interface of XLPE / EPR (**1**) and XLPE / EPDM (**2**) unaged samples (x_P = 0.30 mm, E_{app} = 10 kV/mm)

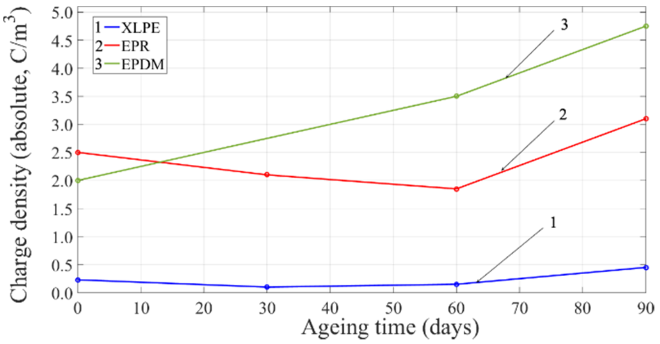

Fig. 47. Variation of the average charge density with the ageing time, for XLPE (1), EPR (2) and EPDM (3) samples (E_{app} = 15 kV/mm)

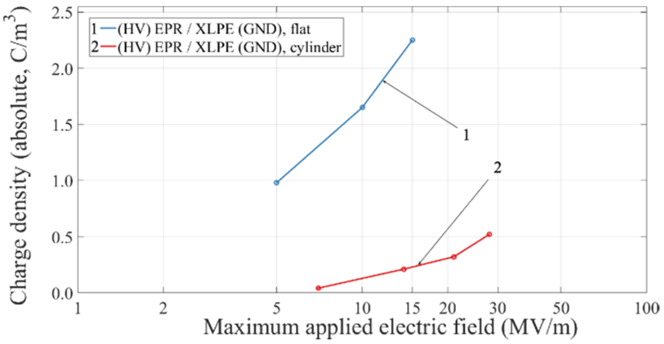

Fig. 48. Variation of the average charge density with the maximum applied electric field, for EPR / XLPE unaged samples with flat (1) and cylindrical (2) geometry, at 10 s after removing the voltage (EPR connected at HV)

The conclusions of Chapter 7 are:

- The unaged samples show relatively smooth surfaces, without open pores, craters, etc. A distinct area of interface between XLPE and EPR can be observed (of approx. 0.5 μm).
- Under the action of heat, the DC cable joints insulations (XLPE, EPR, EPDM) molecules fracture and interact with oxygen, leading to the appearance of polar by-products and / or charged with electrical charges. Analysis of the degradation of EPR and EPDM samples by FTIR showed the presence of a higher number of residual compounds in EPR and higher concentration of oxidized groups in the case of EPDM than in the case of EPR.
- The thermal and electrical stresses to which the samples from XLPE, EPR, XLPE / EPR, EPDM and XLPE / EPDM were subjected to led to important modifications of the electrical properties (conductivity and electrical permittivity). The electrical conductivity values decrease with the measurement duration and increase with the value of the applied electric field and with the ageing time. The permittivity values decrease – with the ageing time – for the XLPE and EPDM samples and increase for EPR samples. These variations are, in percentage, smaller than those of the electrical conductivity.
- The distribution of ρ_v depends on the nature of the sample, on the value and the application of the voltage, on the temperature, etc. In the presence of applied voltage, the increase of E_{app} leads to the increase of ρ_v in the vicinity of electrodes. After the voltage is removed, the maximum values of ρ_v, located in the vicinity of the electrodes, move towards the inside of the samples. These displacements are greater for higher values of E_{app}.
- The values of ρ_v have changed, following ageing, in all samples. $\rho_{v,avg}$ increases with E_{app} (faster for E_{app} > 15 kV/mm for the unaged samples and at lower values of E_{app} in the case of the aged samples). For the XLPE and EPR samples, at the beginning of the thermal stress (first 30 days, respectively first 60 days) the values of $\rho_{v,avg}$ decrease, then increase and after 90 days exceed the values of $\rho_{v,avg}$ corresponding to the unaged samples. For EPDM samples, the values of $\rho_{v,avg}$ increase continuously with the duration of ageing.
- In the case of flat multi-layered samples, during voltage application, ρ_s accumulates at the XLPE / EPR interface, whose density depends on the value of E_{app} and which decreases over time. After removing the voltage, ρ_s changes its polarity quickly (in 1 minute) and decreases slightly (but does not cancel even after 1 hour). On the other hand, the way the electrodes are connected influences the accumulation of space charge. When XLPE is connected to the HV electrode, ρ_v in the vicinity of both electrodes is of positive polarity, and the space charge in the vicinity of the interface is of negative polarity. If the EPR layer is connected to the HV electrode, the ρ_v in the vicinity of both electrodes is of negative polarity, and the space charge in the vicinity of the interface is of positive polarity.

- The space charge density accumulated in the samples also depends on their manufacturing technology; thus, in EPR / XLPE cylindrical samples manufactured using the triple-extrusion method, the average residual average charge density is lower (0.15 C/m^3 for an applied field of 10 kV/mm) than in the case of EPR / XLPE flat samples (or EPDM / XLPE) manufactured by pressing (1.6 C/m^3 for an applied field of 10 kV/mm).
- The insulation materials used for the cable joints must have the lowest possible value of space charge accumulated in their operation. The purity of the basic materials and the manufacturing technology must be improved. Those materials that have smaller variations of ρ_v and implicitly of $\rho_{v,avg}$ should be used, respectively between the studied materials (EPR and EPDM) it is preferable to use EPDM.
- The results in this chapter successfully answered Hypothesis H1 by showing that the thermal ageing duration has a negative effect on the long term electrical properties of cable joint insulations which, in the case of multi-layered samples, was shown to have negatively affected the values of the surface charge density at the interface layer.
- The results in this chapter answered Hypothesis H2 by showing that the thermal ageing duration has a direct negative effect on the accumulation (residual charge density results) and distribution of space charge (volume charge density results) in cable joint insulations.
- The results in this chapter partially answered Hypothesis H4 by presenting methods of reducing space charge by studying the differences between EPR and EPDM as cable joint insulation materials, including improved insulation manufacturing quality.

Chapter 8. Numerical results

In Chapter 8 are numerical results obtained for the distribution of the electric field for flat and cylindrical multi-layered structures (modelling the cable – joint insulation) and for a cable joint design, using as input data the values obtained experimentally (permittivity, conductivity and density of space charge) in Chapter 7. The unanswered part of Hypothesis H4 (regarding improved cable joint design) and Hypothesis H3 (regarding increased electric stresses as main effect of space charge) are answered in this Chapter.

8.1. Electrical conductivity

In the case of multi-layered samples, in order to determine the value of the surface charge density, it is necessary to know the values of the permittivities and electrical conductivities of the constituent layers. Because the empirical relations proposed by various authors (see §4.5.1) have the disadvantage that the calculated values of σ differ quite a lot from those determined experimentally, for values of E ranging between 1 and 30 kV/mm and T between 30 and 70 °C, here, the new empirical expression proposed in Chapter 4, respectively in eq. (4.36), is used and is shown to be more efficient for XLPE, EPR and EPDM. The parameters of eq. (4.36) are determined for the materials from experimental results by choosing sets of {(E, T)} experimental data and by using the MATLAB software with the *fsolve* function from the *Optimization Toolbox* package. For brevity, eq. (4.36) is presented again below:

$$\sigma(E,T) = A \cdot \exp\left(-\frac{E_a}{k_B \cdot T}\right)\frac{\sinh\left((a \cdot T + b) \cdot \ln|E|\right)}{|E|^{\alpha}} \tag{4.36}$$

where A, E_a, a, b and α are the material parameters required to be determined.

8.2. Computation of the electric field

The numerical computation of the electric field was performed using the finite element method in the COMSOL Multiphysics software, the system of equations being solved with the direct factorization method by the MUMPS solver integrated in COMSOL Multiphysics.

A number of three different computational domains have been considered, respectively:

- A flat samples domain (presented in detail in §8.3.1.1 and in fig. 49), in which the electric field distribution was determined in Electrostatics (abbreviated as ES). In COMSOL, the physics interface for the study was Electrostatics of the AC/DC module.
- A cylindrical samples domain (presented in detail in §8.3.1.2 and in fig. 50), in which the electric field distribution was determined in Electrostatics, in Electroquasistatics (abbreviated as EQS) and at Steady Electric Currents (abbreviated as EC). In COMSOL, the physics interface was Electric Currents (in Time Domain) of the AC/DC module.
- A cable joint model (presented in detail in §8.3.1.3 and in figs. 51 and 52), in which the electric field distribution was determined from a coupled Steady Electric Currents and Heat Transfer at steady state. In COMSOL, the physics interfaces were Electric Currents and Heat Transfer in Solids, with Electromagnetic heat and Temperature couplings.

For the Cable joint, the combined computation of the electric field and temperature was performed on a cable joint design courtesy of NKT (according to fig. 52, [46], [103] and [300]), that, for the purposes of the computations, has a length of 1.5 m, thickness 68 mm, is realized from the joining of two cables with an Aluminium conductor (diameter 10 mm), inner semicon. layer (1.5 mm), XLPE insulation (8 mm) and outer semicon. layer (1.5 mm). The joint has a connector area (30 mm × 0.4 m), a joint inner semicon. layer (3 mm), insulation layer of EPR (of variable thickness, maximum 11 mm in the connector area) and a joint outer semicon. layer (of variable thickness, from 4.5 mm at the connector up to 11.5 mm at the extremities).

For this cable joint, the influence of a *Field Grading Material* (or FGM) on the values of the electric field and the surface charge density at the interface between the joint insulation and the cable insulation was studied, and two cases were considered, respectively when there is a continuous layer of FGM that extends along the entire length of the cable joint and that joins the outer semiconductor layer of the cable joint with the inner semiconductor layer of the cable joint (with a thickness of 4 mm for the distance between the two cable joint semiconductor layers and a thickness of 1 mm over the connector area) and when there is no FGM layer, with the respective area considered as part of the joint insulation.

Also, for this cable joint, the influence of the presence of cavities in the joint's insulation was discussed in a separate section of the Chapter. For some of the computations performed in the thesis, a cavity of diameter D_{cav} = 100 μm filled with air at standard pressure and variable temperature was considered, and the dielectric strength of air in DC was equal to $E_{br} = \delta_{air} \cdot 7.86$ kV/mm. If the local value of the electric field at point P_c inside the cavity is higher than the local value of the dielectric strength of air (E_{br}) then it was considered that there is a local breakdown that leads to PD inception and / or intensification, to the initiation and development of electrical trees etc. (as discussed in Chapter 3).

The computations on the cable joint were performed for the cable located with the center at 2 m in the ground, below 30 cm of cable backfill with higher thermal properties than of the soil (more efficient dissipation of losses), and the top of the soil as well as the temperature of the soil at a distance of 2 m all around the center of the cable joint is considered to be at the temperature T = 30 °C. The conductor was set to the applied voltage U_{app} = 50 kV and the heat source is considered to be the Joule losses, transmitted outside by conduction.

The computational domain of the cable joint was simplified to a two dimensional structure of the shape considered in fig. 53 with symmetry considered around the axis of rotation (r = 0, fig. 53) and about a plane that is passing through the middle of the connector (z = 0.7 m, fig. 53).

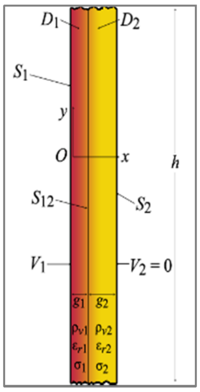

Fig. 49. Flat samples computational domain

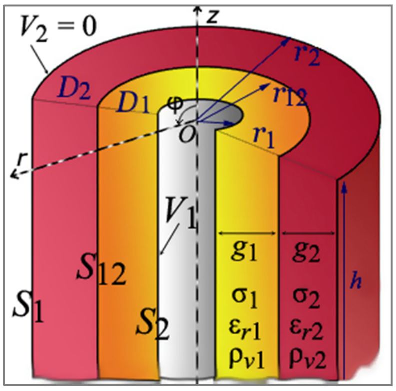

Fig. 50. Cylindrical samples computational domain

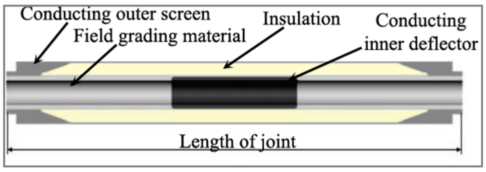

Fig. 51. Cable joint design, after [46]

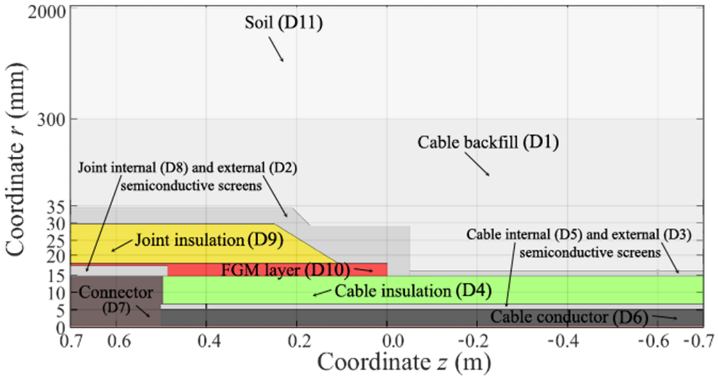

Fig. 52. Cable joint model geometry

For all three distinct computational domains (flat, cylindrical and cable joint), and for all the electric field regimes, it was considered that the magnetic effects are negligible.

The material properties are as follows:

- For flat samples, the values of electrical conductivity and relative permittivity have been determined experimentally at $T = 30$ °C and $E_{app} = 10$ kV/mm, respectively at $f = 50$ Hz.
- For cylindrical samples, the values of the relative permittivity ($f = 50$ Hz) used for computation are those presented in Table 1, at different temperatures. Electrical conductivity values were computed with eq. (4.36).
- For the cable joint model, the values of the material properties for all the subdomains were determined experimentally, computed with empirical expressions or taken from the literature. The electrical conductivity of the FGM layer was considered to be varying only with the electric field, the electrical conductivities of the insulation layers of the cable and the cable joint were considered to be varying with the electric field and the temperature (according to eq. (4.36)), the relative permittivities of the insulation layers of the cable and the cable joint were considered to be varying with temperature ($f = 50$ Hz), and constant values were considered for the rest of the dielectric and thermal properties.

8.3. Flat samples

The electric field distributions obtained on flat samples (geometry model presented in fig. 49) are further divided into variations with the type of material, influence of the applied electric field and of the ageing time.

Figure 51 shows the variation with the coordinate x of the electric field E computed in ES for $T = 30$ °C and $E_{app} = 5$ kV/mm for XLPE / EPR and XLPE / EPDM unaged multi-layered samples, where XLPE is the material considered for the subdomain $D1$ and EPR or EPDM is the material considered for the subdomain $D2$. It was also considered that $\rho_v = 0$

everywhere in the sample and, at the interface, $\rho_s = 0$. The maximum value obtained for E is in the subdomain $D1$ (XLPE) and this value is 8 % higher (5.6 MV/m compared to 6.15 MV/m) for XLPE / EPDM samples than for XLPE / EPR samples. This is due to the different permittivities of the material in the $D2$ subdomain, respectively to the fact that $\varepsilon_{r,EPDM} > \varepsilon_{r,EPR}$.

In the presence of ρ_s at the interface (on surface $S12$), the electric field distribution changes; ρ_s was determined to be higher for all cases for XLPE / EPR samples than for XLPE / EPDM samples. The values of ρ_s determined by computation (of order mC/m^2) determine an increase of E of approx. 2 times in XLPE (from 5.8 to 11.7 MV/m) and a decrease of 4 times in EPR (from 4.4 to 1.1 MV/m).

If a volume space charge density ρ_v also exists (determined experimentally in Chapter 7), the distribution of the electric field changes even more. For XLPE / EPR samples, the presence of ρ_v modifies the values of the electric field, increasing it both in XLPE (E = 20 MV/m at the point of coordinate x = 0.12 mm) and in EPR (E = -8 MV/m at the point of coordinate x = 0.79 mm, respectively in the vicinity of GND). For XLPE / EPDM samples, in XLPE in the vicinity of the HV electrode E decreases and changes its polarity (reaching -4 MV/m), and towards the interface E increases from 6 MV/m (initially) to 7 MV/m. In EPDM, at the interface, the value of E is higher up to 1.3 times (3 MV/m compared to 2.2 MV/m initially), has a maximum (E = 4.5 MV/m) in the area of coordinate x = 0.65 mm and decreases and changes its polarity in the area of GND (reaching E = -4 MV/m).

The simultaneous presence of surface charge density and volume charge density leads to an even greater intensification of the electric field, for XLPE / EPR samples its values reaching 25.3 MV/m in the XLPE layer and -12 MV/m in the EPR layer, and for XLPE / EPDM samples its values reaching 10 MV/m in the XLPE layer and 6.5 MV/m in the EPDM layer.

The modification of the applied electric field E_{app} leads to the modification of the space charge density distribution and to the modification of the electric field distribution, both in the presence and in the absence of applied voltage. For XLPE / EPR samples, in Voltage-ON, E changes more for E_{app} > 5 kV/mm (fig. 52). This may be due to the separation of space charge near the electrodes and at the XLPE / EPR interface. The existence of a non-zero space charge density after removing the voltage causes the residual electric field to have significant non-zero values, especially for E_{app} > 5 kV/mm (fig. 53). The variation of the maximum value of the electric field E_{max} as a function of E_{app}, during voltage application, is presented in fig. 54, and the variation with the measurement time of the coordinate x of the point where E takes the maximum value is presented in fig. 55. It is observed (fig. 54) that E_{max} depends on E_{app} and that is significantly higher than it (for E_{app} = 15 kV/mm, E_{max} reaches up to 89 kV/mm). For E_{app} < 15 kV/mm, E_{max} increases in the first 10 minutes and remains quasi-constant until the end of the measurement time. For E_{app} = 15 kV/mm, E increases up to a maximum in approx. 10 minutes and then decreases to 85 % of the maximum. From fig. 55 it is observed that, regardless of the value of E_{app}, E_{max} is found in the central area of XLPE.

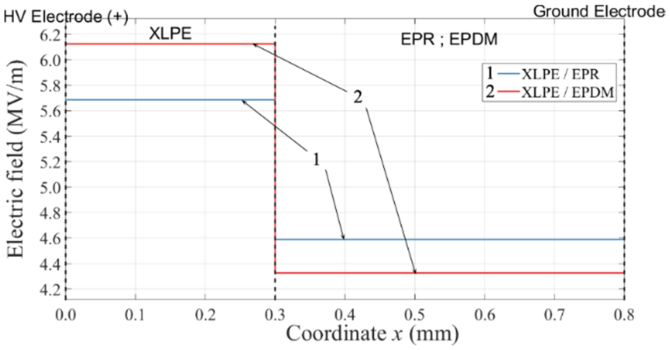

Fig. 51. Variation of the electric field with the coordinate x during voltage application, for XLPE / EPR (1) and XLPE / EPDM (2) unaged samples (ES, Voltage-ON, E_{app} = 5 kV/mm, T = 30 °C, $\rho_v = \rho_s = 0$)

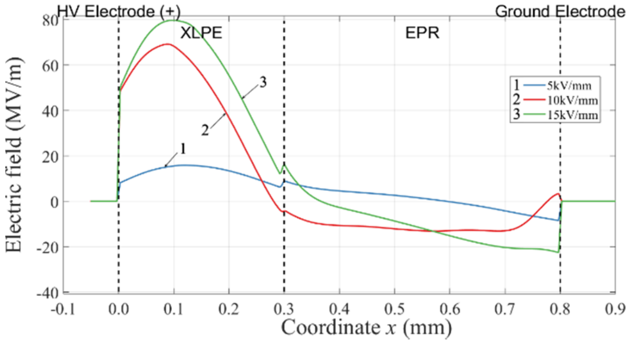

Fig. 52. Variation of the electric field with the coordinate x for XLPE / EPR unaged samples at an hour after voltage application, for E_{app} = 5 (1), 10 (2) and 15 (3) kV/mm (ES, t = 3600 s, Voltage-ON, $\rho_v \neq 0$, $\rho_s = 0$)

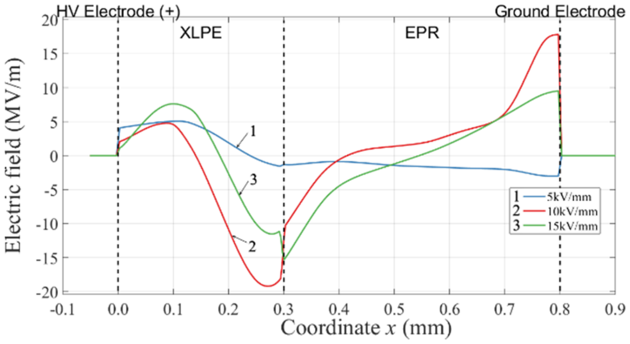

Fig. 53. Variation of the electric field with the coordinate x for XLPE / EPR unaged samples at 300 s after removing the voltage, for E_{app} = 5 (1), 10 (2) and 15 (3) kV/mm (ES, t = 300 s, Voltage-OFF, $\rho_v \neq 0$, $\rho_s = 0$)

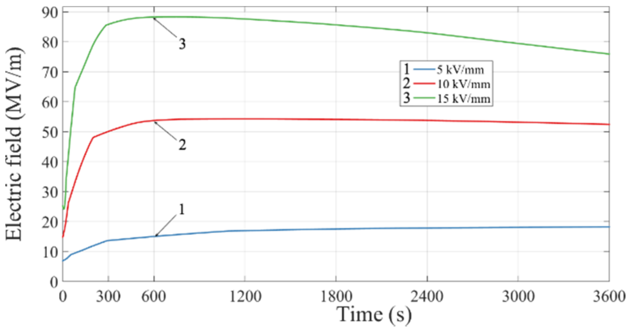

Fig. 54. Variation of the maximum value of the electric field at different measurement times during voltage application, for XLPE / EPR unaged samples, for E_{app} = 5 (1), 10 (2) and 15 (3) kV/mm (Voltage-ON, $\rho_v \neq 0$, $\rho_s = 0$)

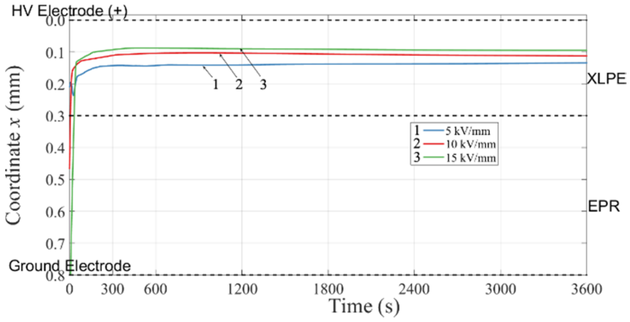

Fig. 55. Variation of the coordinate x of the maximum value of the electric field at different measurement times during voltage application, for XLPE / EPR unaged samples, for E_{app} = 5 (1), 10 (2) and 15 (3) kV/mm (Voltage-ON, $\rho_v \neq 0$, $\rho_s = 0$)

For XLPE / EPDM samples, in Voltage-ON, E change proportionally with E_{app} (fig. 56), the separation of space charge near the electrodes and at the XLPE / EPDM interface leading to the local increase or decrease of the electric field. At the same time, the existence of a non-zero space charge density after removing the voltage causes the residual electric field to have significant non-zero values, especially for the cases where $E_{app} > 5$ kV/mm (fig. 57). The variation of E_{max} as a function of E_{app}, during voltage application, is presented in fig. 58, and the variation with the measurement time of the coordinate x of the point where E takes the maximum value is presented in fig. 59. E_{max} depends on E_{app} (fig. 58) and, for values of $E_{app} < 15$ kV/mm, it is found, initially, in the middle of the sample (in the EPDM area, at $x_P \approx 0.45$ mm) and it moves towards the interface during the measurement. For $E_{app} = 15$ kV/mm the maximum value E_{max} is found in the XLPE area of the sample (at $x_P \approx 0.15$ mm) for the whole measurement duration (fig. 59). After removing the voltage, near the ground electrode the residual values of E depend on the value of E_{app} and, regardless of the value of E_{app}, E is not cancelled until the end of the measurement.

The distribution of the electric field E is influenced by the ageing time for the samples, both in the presence and in the absence of applied voltage (figs. 60 and 61), due to the changes brought by the new space charge density distribution with the ageing time. In the presence of applied voltage (Voltage-ON), the values of the electric field increase in the vicinity of both electrodes in the aged samples compared to the unaged samples (fig. 60). If the applied voltage is removed, at any instant t the values of the residual electric field near the electrodes are higher in the aged samples than in the unaged samples (fig. 61).

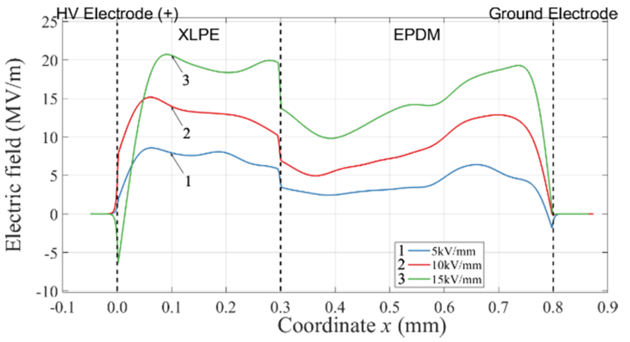

Fig. 56. Variation of the electric field with the coordinate *x* for XLPE / EPDM unaged samples at 2400 s after voltage application, for E_{app} = 5 (**1**), 10 (**2**) and 15(**3**) kV/mm (ES, *t* = 2400 s, Voltage-ON, $\rho_v \neq 0$, $\rho_s = 0$)

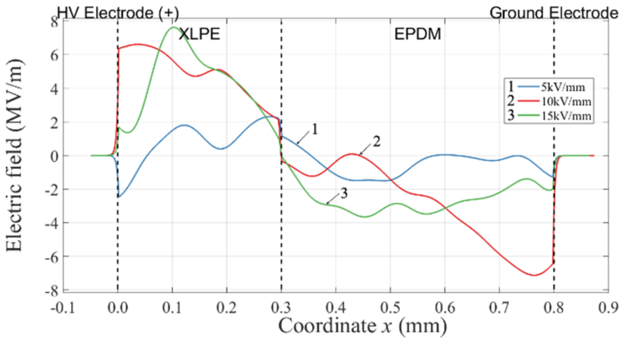

Fig. 57. Variation of the electric field with the coordinate *x* for XLPE / EPR unaged samples at 60 s after removing the voltage, for E_{app} = 5 (**1**), 10 (**2**) and 15 (**3**) kV/mm (ES, *t* = 60 s, Voltage-OFF, $\rho_v \neq 0$, $\rho_s = 0$)

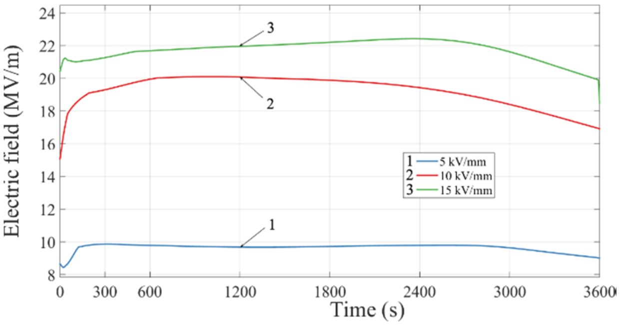

Fig. 58. Variation of the maximum value of the electric field at different measurement times during voltage application, for XLPE / EPDM unaged samples, for E_{app} = 5 (**1**), 10 (**2**) and 15 (**3**) kV/mm (Voltage-ON, $\rho_v \neq 0$, $\rho_s = 0$)

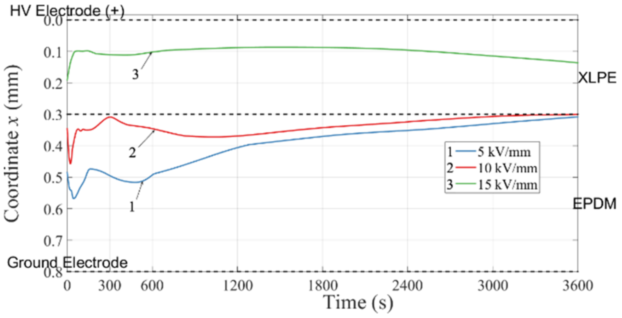

Fig. 59. Variation of the coordinate *x* of the maximum value of the electric field at different measurement times during voltage application, for XLPE / EPDM unaged samples, for E_{app} = 5 (**1**), 10 (**2**) and 15 (**3**) kV/mm (Voltage-ON, $\rho_v \neq 0$, $\rho_s = 0$)

During voltage application, the variation with the measurement time of $E_{\max}$ and of the position of $E_{\max}$ are presented in figs. 62 – 63. $E_{\max}$ takes higher values in the aged samples than in the unaged samples (fig. 62) and it increases in the first 15 minutes and then remains, practically, constant until the end of the measurement time. Regardless of the ageing time, $E_{\max}$ is present in the XLPE layer, respectively close to its center (around coordinate x_P = 0.10 – 0.15 mm, fig. 63). After removing the voltage, near the ground electrode the residual values of *E* decrease over time, regardless of the value of E_{app}, and are not cancelled.

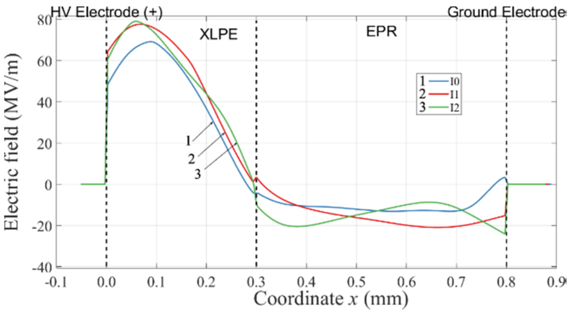

Fig. 60. Variation of the electric field with the coordinate *x* at an hour after voltage application, for unaged (I0, **1**) and aged for 30 days (I1, **2**) and 60 days (I2, **3**) XLPE / EPR samples (ES, *t* = 3600 s, Voltage-ON, E_{app} = 10 kV/mm, $\rho_v \neq 0$, $\rho_s = 0$)

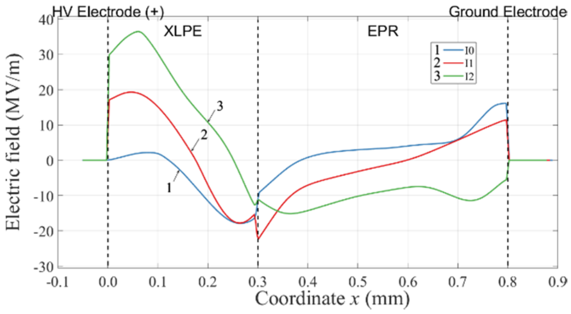

Fig. 61. Variation of the electric field with the coordinate *x* at 600 s after removing the voltage, for unaged (I0, **1**) and aged for 30 days (I1, **2**) and 60 days (I2, **3**) XLPE / EPR samples (ES, *t* = 600 s, Voltage-OFF, E_{app} = 10 kV/mm, $\rho_v \neq 0$, $\rho_s = 0$)

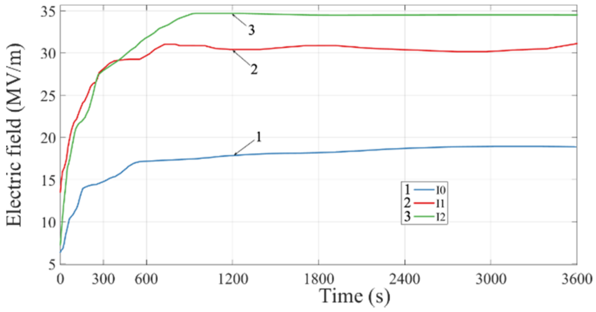

Fig. 62. Variation of the maximum value of the electric field at different measurement times during voltage application, for unaged (I0, **1**) and aged for 30 days (I1, **2**) and 60 days (I2, **3**) XLPE / EPR samples (Voltage-ON, E_{app} = 5 kV/mm, $\rho_v \neq 0$, $\rho_s = 0$)

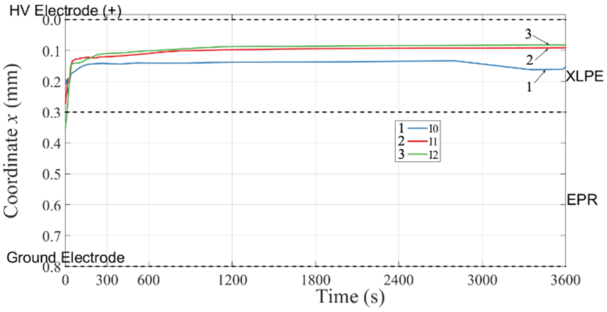

Fig. 63. Variation of the coordinate *x* of the maximum value of the electric field at different measurements time during voltage application, for unaged (I0, **1**) and aged for 30 days (I1, **2**) and 60 days (I2, **3**) XLPE / EPR samples (Voltage-ON, E_{app} = 5 kV/mm, $\rho_v \neq 0$, $\rho_s = 0$)

8.4. Cylindrical samples

The *E* distributions on cylindrical samples (fig. 50) were obtained in ES, in EQS and in EC. In ES, the presence of ρ_v and ρ_s was considered, both determined experimentally for different U_{app} (25, 50, 75 and 100 kV), at *T* = 30 °C. In EQS, the presence of ρ_s was considered, determined by computation for different U_{app} (25, 50, 75 and 100 kV) and *T* (30 – 90 °C).

In ES, in the absence of space charge ($\rho_v = \rho_s = 0$), *E* varies with coordinate *r* depending on the applied voltage and the electric permittivities of the subdomains (*D*1 and *D*2) (fig. 64). For subdomain *D*1, *E* is more intense in EPR than in EPDM (the maximum value, near the HV electrode, is 6.6 MV/m (EPR) compared to 6.5 MV/m (EPDM)). In subdomain *D*2 the maximum value of the electric field (near the interface) is more intense by 12 % in the case of the EPDM / XLPE sample (6.3 MV/m) compared to the EPR / XLPE sample (5.6 MV/m). This behaviour is due to the values of ε_r which are higher for EPDM (3.2) than for EPR (2.8).

Increasing the applied voltage leads to the modification of the electric field distribution, both in its presence (fig. 65) and in its absence (fig. 66). Thus, in the presence of applied voltage, for U_{app} < 100 kV, the values of the electric field *E* increase with the increase of U_{app} (fig. 65). For U_{app} = 100 kV, *E* has a maximum (43 kV/mm) near GND (fig. 65).

The variation with the measurement time of the maximum value of the electric field $E_{\max}$ is presented in fig. 67, and the variation with the measurement time of the coordinate *r* of the point where *E* takes the maximum value is presented in fig. 68; $E_{\max}$ depends on the applied voltage: is constant for U_{app} < 100 kV and increase over time for U_{app} = 100 kV (fig. 67). For values of $U_{app} \leq 50$ kV, $E_{\max}$ is found in the middle of the sample (in the EPR area, $r_P \approx 10.00$ mm) throughout the measurement, and for U_{app} > 50 kV $E_{\max}$ is found, initially, in the middle of the sample, then moves, over time, to the ground electrode (fig. 68).

The existence of $\rho_v \neq 0$ causes the residual electric field to retain significant values, even after removing the applied voltage. For U_{app} = 100 kV, 600 s after removing the voltage and near GND, *E* = -37 kV/mm. Throughout the bulk of the sample, the values of *E* depend on those of U_{app}, and near GND *E* increases over time to a higher value, the higher U_{app} values are.

In EQS (as well as in EC), the electric field distribution is also influenced by the variation of the electrical conductivity with the temperature and the electric field. The electrical conductivity for a EPR / XLPE sample, at *T* = 30 °C and U_{app} = 25 kV, is higher in EPR than in XLPE, decreases with the increase of *r*, is higher in the vicinity of the HV electrode (*r* = 8 mm) – where the electric field is more intense – and that, over time, the values of σ increase in EPR (maximum value increases 1.2 times from 8 to 9.5 fS/m) and decrease in XLPE (maximum value decreases 1.6 times from 3.5 to 2.1 fS/m).

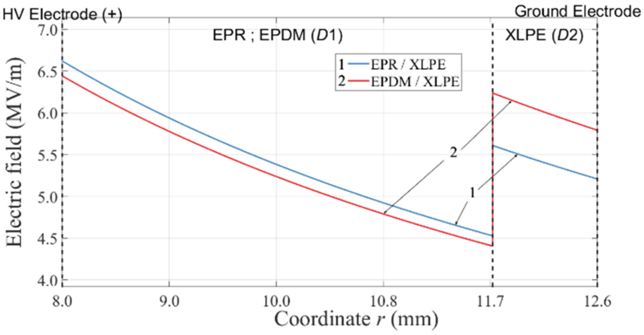

Fig. 64. Variation of the electric field with the coordinate *r* during voltage application, for EPR / XLPE (1) and EPDM / XLPE (2) unaged samples (ES, $T = 30$ °C, $U_{app} = 25$ kV, $\rho_v = 0$, $\rho_s = 0$)

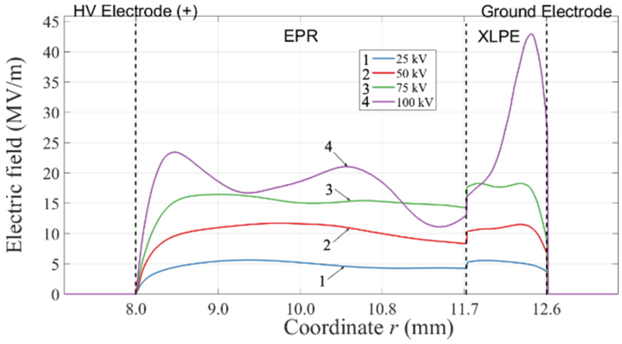

Fig. 65. Variation of the electric field with the coordinate *r* for EPR / XLPE unaged samples, at 1 hour after voltage application, for $U_{app} = 25$ (1), 50 (2), 75 (3) and 100 (4) kV (ES, $t = 3600$ s, Voltage-ON, $\rho_v \neq 0$, $\rho_s = 0$)

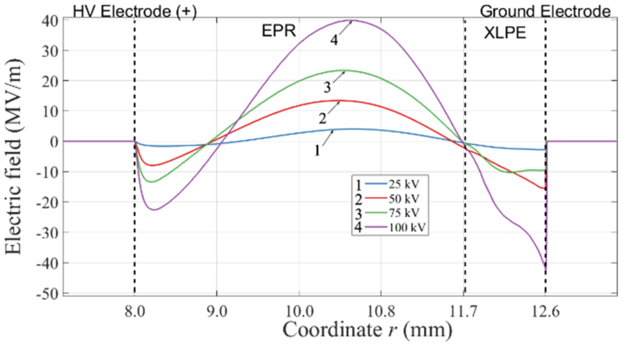

Fig. 66. Variation of the electric field with the coordinate *r* for EPR / XLPE unaged samples, at 600 s after removing the voltage, for $U_{app} = 25$ (1), 50 (2), 75 (3) and 100 (4) kV (ES, $t = 600$ s, Voltage-OFF, $\rho_v \neq 0$, $\rho_s = 0$)

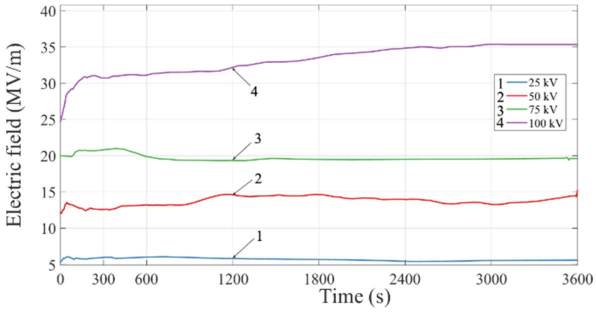

Fig. 67. Variation of the maximum value of the electric field at different measurement times during voltage application, for EPR / XLPE unaged samples, at $U_{app} = 25$ (1), 50 (2), 75 (3) and 100 (4) kV (Voltage-ON, $\rho_v \neq 0$, $\rho_s = 0$)

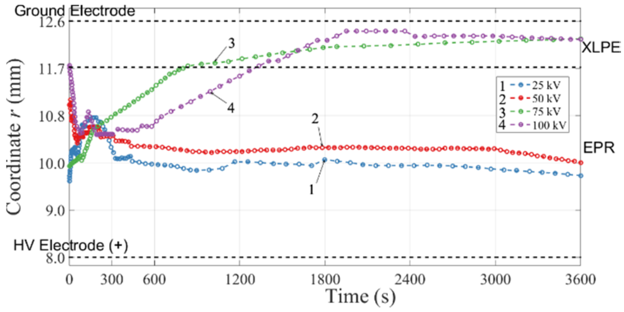

Fig. 68. Variation of the coordinate *r* of the maximum value of the electric field at different measurement times during voltage application, for EPR / XLPE unaged samples at $U_{app} = 25$ (1), 50 (2), 75 (3) and 100 (4) kV (Voltage-ON, $\rho_v \neq 0$, $\rho_s = 0$)

The electrical conductivity for a EPR / XLPE sample at $T = 30$ °C and $t = 3600$ s, increases with increasing applied voltage, both in EPR (near HV electrode approx. 2.1 times, from 9.2 to 19.5 fS/m) and in XLPE (near the interface approx. 3.7 times, from 2.2 to 8.1 fS/m).

The electrical conductivity for a EPR / XLPE sample at $U_{app} = 50$ kV and $t = 3600$ s, increases with increasing temperature, both in EPR (near HV electrode almost 2.5 orders higher, from 14 fS/m to 4 pS/m) and in XLPE (near the interface almost 4 times, from 5 to 20 fS/m).

The distribution of the electrical conductivity also depends on the type of material (different parameters values for the $\sigma(T,E)$ expression for XLPE, EPR and EPDM). The values of σ are higher, in both subdomains, for the case of EPR / XLPE than for EPDM / XLPE.

Because in each subdomain σ varies with E and T, the surface charge density ρ_s at the interface between the subdomains (on S_{12}) also changes. The variation of ρ_s with the measurement time, for EPR / XLPE samples, at different values of T for a value of E (corresponding to $U_{app} = 50$ kV) is shown in fig. 69, ***a***. It is found that the surface charge density ρ_s tends to a maximum value $\rho_{s,max}$, corresponding to steady state, and that this value is reached at a moment τ_{max} that decreases with increasing temperature: for $T = 30$ °C, $\tau_{max} = 6400$ s, and for $T = 90$ °C, $\tau_{max} = 200$ s.

The variation of ρ_s with the measurement time, for EPR / XLPE samples, at different values of E for $T = 30$ °C is presented in fig. 69, *b*. It is found that the surface charge density ρ_s tends to a maximum value $\rho_{s,max}$, corresponding to steady state, and that this value is reached at a moment τ_{max} that decreases with increasing the applied voltage: for $U_{app} = 25$ kV, $\tau_{max} = 10700$ s, and for $U_{app} = 100$ kV, $\tau_{max} = 5520$ s. On the other hand, the temperature variation of the surface charge density has a more pronounced effect than the electric field variation of the surface charge density, respectively that $\rho_{s,max}$ increases faster with increasing temperature than with increasing electric field.

The variation of ρ_s with the measurement time, at $T = 30$ °C and $U_{app} = 25$ kV, is presented in fig. 69, *c*, for EPR / XLPE (fig. 69, *c*, curve **1**) and EPDM / XLPE (fig. 69, *c*, curve **2**). The surface charge density increases over time to a maximum, $\rho_{s,max}$, which is equal to 0.18 mC/m^2 for the EPR / XLPE samples and 0.08 mC/m^2 for the EPDM / XLPE samples. This is due to the higher values of the electrical conductivity of EPR than of EPDM. It is also observed that the time at which the surface charge density value reaches its maximum is longer for the EPDM / XLPE samples (9 hours) than for EPR / XLPE samples (7 hours).

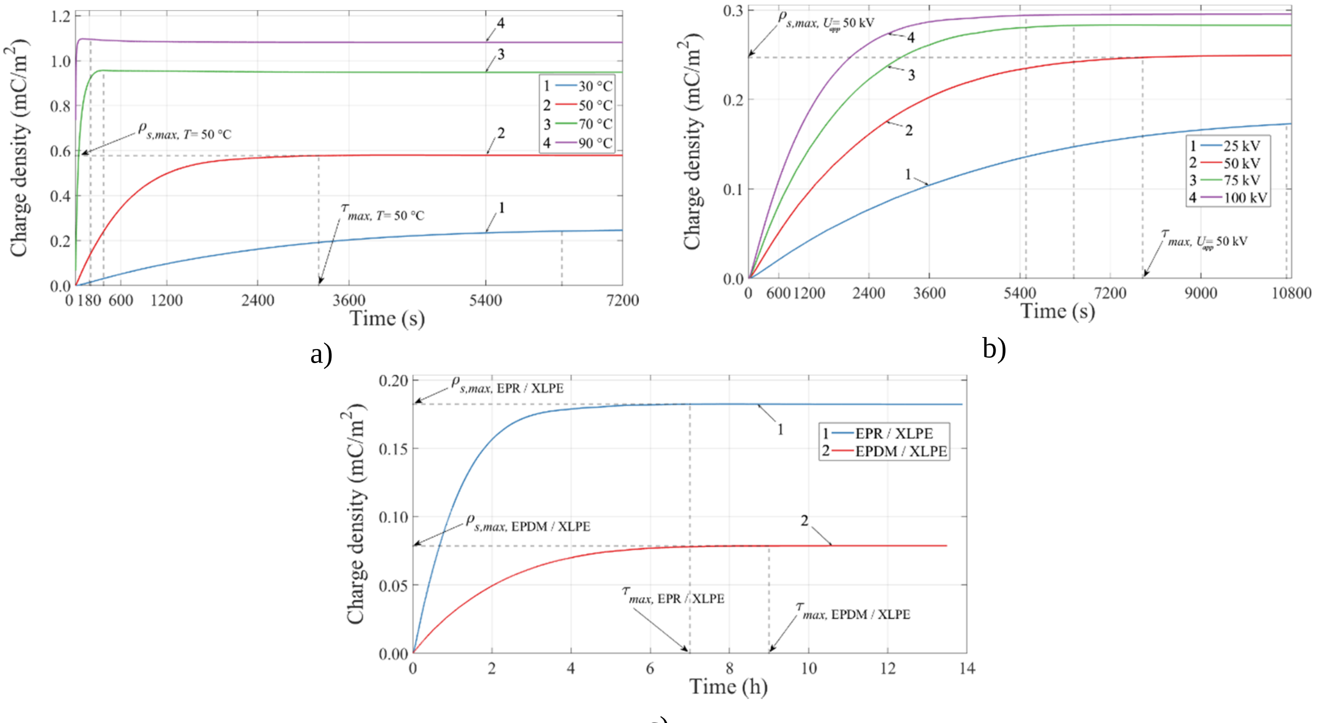

a)

b)

c)

Fig. 69. Variation of the surface charge density with the measurement time, during voltage application, for EPR / XLPE unaged samples (**a** and **b**) and for EPR / XLPE and EPDM / XLPE unaged samples (**c**),
a. at $T = 30$ (**1**), 50 (**2**), 70 (**3**) and 90 °C (**4**) (EQS, Voltage-ON, $U_{app} = 50$ kV)
b. at $U_{app} = 25$ (**1**), 50 (**2**), 75 (**3**) and 100 kV (**4**) (EQS, Voltage-ON, $T = 30$ °C)
c. for EPR / XLPE (**1**) and EPDM / XLPE (**2**) unaged samples
(EQS, Voltage-ON, $T = 30$ °C, $U_{app} = 25$ kV)

8.5. Cable joint

For the cable joint, the computation of the electric field *E* was performed for the joint geometry presented in fig. 52, where, initially, between the insulation layer of the cable joint (EPR, subdomain *D*9) and the insulation layer of the cable (XLPE, subdomain *D*4) there is no interposed FGM-type material, respectively that subdomain *D*10 is part of subdomain *D*9.

The distribution of equipotential lines are presented in fig. 70 and the distribution of the electric field in fig. 71. The equipotential lines are denser in the area of the insulation layers near the center of the cable joint (around the connector) and sparse (or not at all) towards the extremities of the cable joint (fig. 70). *E* has higher values in the insulation layer of the cable than in of the joint, where it decreases with the coordinate *r* while in the insulation layer of the joint (above the connector) it increases slightly with coordinate *r* (fig. 71). At the end of the inner semiconductor layer of the joint a local concentration of *E* is observed (fig. 71).

If between the insulation layer of the cable joint and the insulation layer of the cable there is a layer with nonlinear electrical properties (a FGM layer) (subdomain *D*10), the distributions of the equipotential lines (fig. 72) and of the electric field (fig. 73) are modified: the equipotential lines are distributed along the entire length of the insulation layers of the cable and joint (fig. 72), and *E* has lower values in both insulation layers (fig. 73). At the end of the inner semiconductor layer of the cable joint, the local concentration of the electric field (present in fig. 71) no longer exists (fig. 73).

In order to study in more detail the influence of the FGM layer interposed between the insulation layers of the cable and joint, several points and lines were chosen for which local values were obtained or the variation curves of some values were plotted. The spatial location of these points and lines is presented in fig. 74 (points) and fig. 75 (lines).

Table 2 shows the values of the electric field at point *P*3 (near the outer corner of the inner semiconductor layer of the cable joint), considered to be the point where a high local concentration of *E* was observed, in the absence and presence of FGM. The electric field is approx. 25 times higher in the case of absence than the presence of the FGM layer (*E* takes the value 9.63 MV/m in the absence of FGM and only 0.41 MV/m in the presence of FGM).

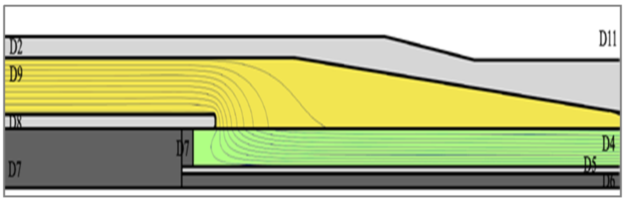

Fig. 70. Spatial distribution of equipotential lines in the area of the cable joint connector, no FGM

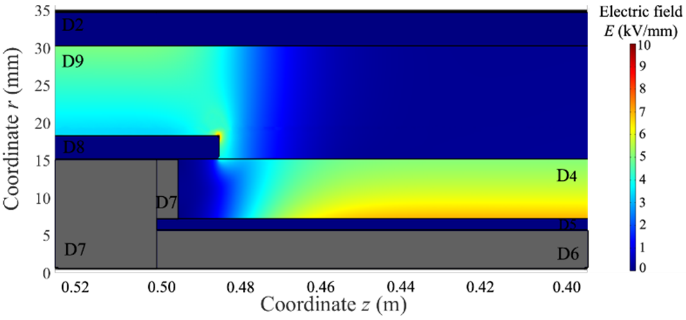

Fig. 71. Spatial distribution of the electric field in the area of the cable joint connector, no FGM

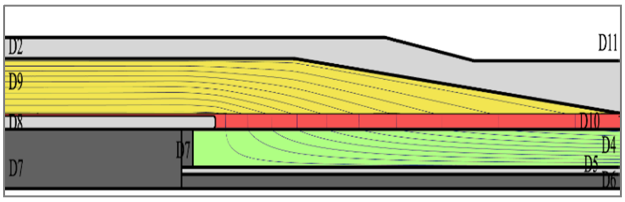

Fig. 72. Spatial distribution of equipotential lines in the area of the cable joint connector, with FGM

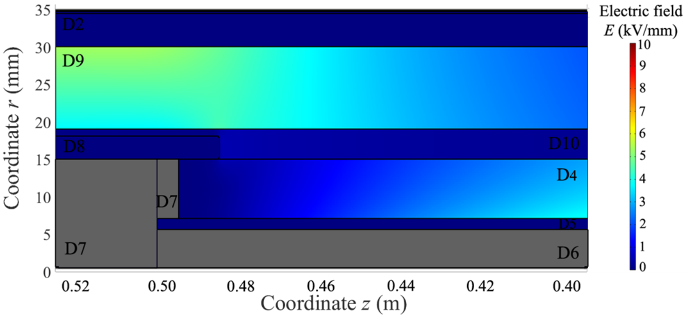

Fig. 73. Spatial distribution of the electric field in the area of the cable joint connector, with FGM

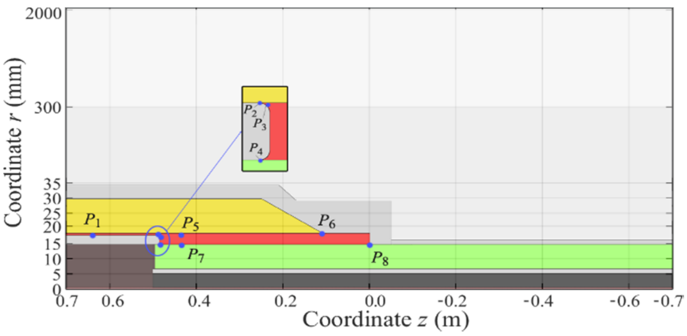

Fig. 74. Location in space of study points

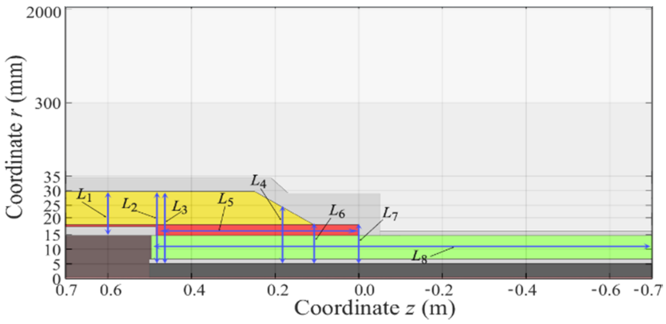

Fig. 75. Location in space of study lines

Table 3 shows the values of the surface charge density ρ_s (determined in EQS at a very large instant as to be considered at steady state) at two points, *P*5 and *P*7, on an imaginary line along the *r*-axis, at $z = 0.45$ m, points *P*5 and *P*7 corresponding to the interfaces between the FGM layer and the insulation layer of the cable (point *P*7) and between the FGM layer and the insulation layer of the cable joint (point *P*5). In the absence of the FGM layer, point *P*5 is considered to be part of the insulation layer of the cable joint, and thus ρ_s at this point is zero. Although the presence of the FGM layer creates a new interface (point *P*5), the surface charge density is higher in the case of absence than presence of the FGM layer. The polarity of the surface charge density is negative in the case without FGM and positive in the case with FGM.

Figure 76, *a*, shows the variation of the electric field *E* for line *L*1 (over the connector), in the absence (fig. 76, *a*, curve **1**) and in the presence of FGM (fig. 76, *a*, curve **2**). The values of *E* increase with the coordinate *r* and are higher in the cable joint insulation (subdomain *D*9) by approx. 7.3 % (at the point of coordinate $r = 29.5$ mm, $E = 5.31$ MV/m compared to 4.95 MV/m) if FGM is present in subdomain *D*10 (fig. 76, *a*, curve **2**) than if the subdomain *D*10 is part of the insulation layer of the cable joint (fig. 76, *a*, curve **1**). The resulting inversion of the electric field profile across the insulation layer of the cable joint (fig. 76, *a*, subdomain *D*9), respectively higher values at the outer insulation shield (at 52 °C) and lower values at the inner insulation shield (63 °C), is expected, considering the temperature gradient drop of 11 °C between the inner and outer shield positions, and, knowing that the DC steady state electric field distribution is determined by the local conductivity of the insulation (which is electric field and temperature dependent) [46].

If at the point P_c of coordinate $r = 29.5$ mm (in the area of maximum values of *E* from fig. 8.58, corresponding to the interface between the insulation of the cable joint and the outer semiconductor layer of the cable joint) there is a cavity of diameter $D_{cav} = 0.1$ mm (according to §8.4), then the dielectric strength of air (according to eq. (8.21) and fig. 8.9), at the value of the temperature at point P_c, has the value $E_{br}(P_c) = 7.205$ MV/m.

Table 2. Values of the electric field at point *P*3

Case	**Electric field *E* (MV/m)**
No FGM	9.63
With FGM	0.41

Table 3. Values of the surface charge density at points *P*5 and *P*7

Case	**Surface charge density ρ_s (μC/m^2)**		
	At point *P*5	At point *P*7	Sum *P*5 + *P*7
No FGM	0	-92.42	-92.42
With FGM	14.99	5.60	20.59

The local electric field inside the cavity is (according to eq. (8.20)) $E(P_c)$ = 7.255 MV/m (in the absence of FGM, (fig. 76, *a*, curve **1**)) and 7.775 MV/m (in the presence of FGM, (fig. 76, *a*, curve **2**)). At this point (P_c), the electric field inside the cavity is sufficient to initiate a local breakdown, regardless of the existence of the FGM. Because P_c is in the vicinity of the outer semicon. layer of the joint, there is a possibility of diffusion of water molecules from the environment, causing the accumulation of space charge particles and producing electrochemical trees, worsening the dielectric properties of the insulation of the joint (see §3.2).

Figure 76, *b*, shows the variation of the electric field *E* for line *L*2 (at 0.05 mm from the end of the inner semicon. layer of the joint, between the cable insulation (subdomain *D*4), the FGM layer (subdomain *D*10) and the cable joint insulation (subdomain *D*9)), in the absence (fig. 76, *b*, curve **1**) and in the presence of FGM (fig. 76, *b*, curve **2**). The values of *E* in the insulation layer of the cable (subdomain *D*4), in the FGM layer (subdomain *D*10) and in the insulation layer of the cable joint (subdomain *D*9) are lower in the presence (fig. 76, *b*, curve **1**) than in the absence of FGM (fig. 76, *b*, curve **2**), except in subdomain *D*9 for the points of coordinate $r > 20$ mm, where the values of *E* are up 22 % higher (4.75 MV/m compared to 3.90 MV/m at the point of coordinate $r = 29.5$ mm).

In the insulation layer of the cable (subdomain *D*4), the values of *E* are 7 – 8.4 times lower in the presence of FGM (fig. 76, *b*, curve **2**); for example, at point P_c of coordinate $r = 15$ mm, $E = 0.5$ MV/m compared to 4.2 MV/m. On the other hand, in the absence of FGM (fig. 76, *b*, curve **1**), *E* presents a maximum around the point of coordinate $r = 17.25$ mm (corresponding to the influence of the corner of the inner semiconductor layer of the cable joint), respectively $E_{\max} = 7.87$ MV/m. The value of $E_{\max}$ decreases to 0.62 MV/m in the absence of FGM (fig. 76, *b*, curve **2**).

Figure 76, *c*, shows the variation of the electric field *E* for line *L*4 (at 300 mm from the end of the inner semiconductor layer of the cable joint, between the insulation of the cable (subdomain *D*4), the FGM layer (subdomain *D*10) and the insulation of the cable joint (subdomain *D*9)), in the absence (fig. 76, *c*, curve **1**) and in the presence of FGM (fig. 76, *c*, curve **2**). It is observed that at this distance from the connector, *E* decreases with the coordinate *r* in all subdomains (while for the positions closer to the connector, *E* increases with the coordinate *r* in the insulation of the cable joint (subdomain *D*9) (see also fig. 76, *a*)).

It is found that the values of *E* in the insulation of the cable (subdomain *D*4) are only 10 % higher in the absence of FGM (fig. 76, *c*, curve **1**) than in the presence of FGM (fig. 76, *c*, curve **2**), respectively 5.90 MV/m compared to 5.76 MV/m at the point of coordinate $r = 10$ mm. Also, in the presence of FGM (fig. 76, *c*, curve **2**), the values of *E* in the insulation of the cable joint (subdomain *D*9) are 2.5 times higher in the absence of FGM (fig. 76, *c*, curve **1**), respectively 0.67 MV/m compared to 0.27 MV/m at the point of coordinate $r = 20$ mm.

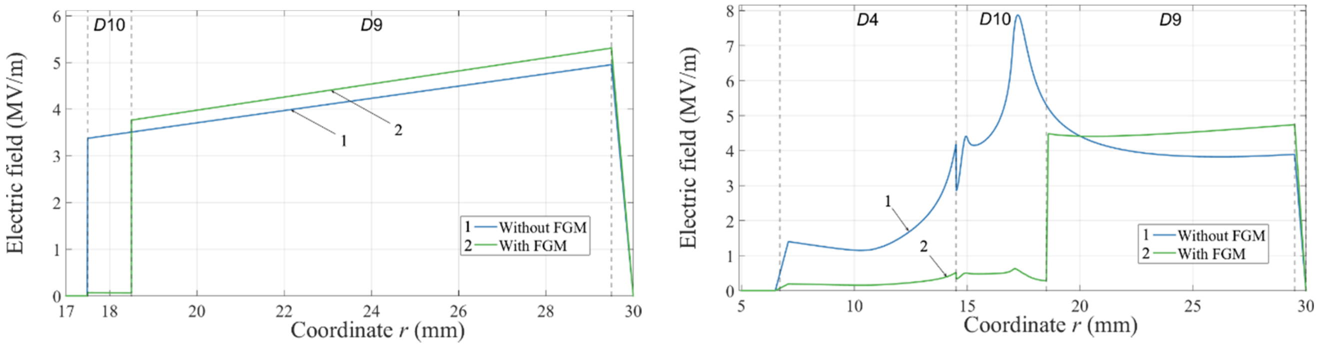

a) b)

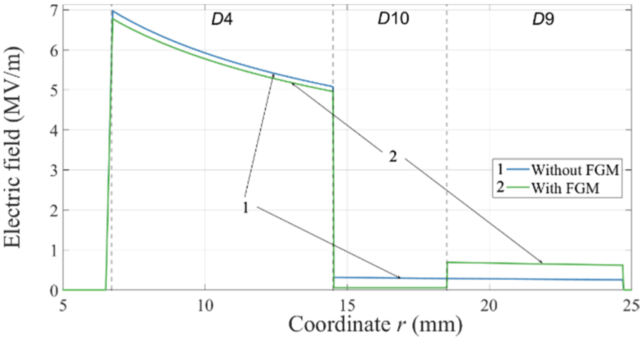

c)

Fig. 76. Variation of the electric field with the coordinate *r*, in the absence (1) and in the presence (2) of the FGM layer: ***a)*** across line *L*1 ; ***b)*** across line *L*2 ; ***c)*** across line *L*4

The conclusions of Chapter 8 are:

- The proposed empirical relationship for determining the electrical conductivity as a function of electric field and temperature is validated experimentally.
- For flat samples, in Electrostatics, the maximum value of the electric field is found in the subdomain of XLPE and is 8 % higher for XLPE / EPDM than for XLPE / EPR samples.
- In the steady state, the presence of a surface charge intensifies the values of *E* in XLPE and decreases them in EPR or in EPDM, the effect on the distribution of *E* is more intense for XLPE / EPR than for XLPE / EPDM flat samples (*E* increases almost 2.2 times in XLPE and decreases almost 4 times in EPR for XLPE / EPR samples and increases almost 1.5 times in XLPE and decreases almost 1.8 times in EPDM for XLPE / EPDM samples).
- The presence of a volume charge density modifies the distribution of the electric field, becoming, locally, more intense up to 4 times in XLPE in the case of XLPE / EPR flat samples and up to 1.25 times in XLPE in the case of XLPE / EPDM flat samples.
- For cylindrical samples, the existence of space charge determines an important change of the electric field distribution, both in the presence and in the absence of applied voltage. In the presence of applied voltage, the values of *E* decrease in the vicinity of the electrodes and increase in the central areas of the samples. When the voltage is removed, the residual values of *E* are reduced over time but they are not cancelled even after one hour.
- The variation of electrical conductivity with *T* has a more pronounced effect than the variation with *E* on the values of ρ_s accumulated at the interface; ρ_s reaches its maximum value faster for higher temperatures than for higher electric field values.
- The higher the electrical conductivity of the constituent materials of the sample, the faster surface charge density accumulates at the interface, and its maximum value is higher. Because $\sigma_{EPR} > \sigma_{EPDM}$, a higher value for the surface charge density accumulates at the interfaces of the EPR / XLPE cylindrical samples than EPDM / XLPE cylindrical samples.
- All of the above results support Hypothesis H3 regarding electric stresses enhancement as effect of space charge, and, as seen in Chapter 3, it leads to joint insulation degradation.
- The incorporation of a FGM layer into the structure of cable joints leads to a lower accumulation of space charge at the interfaces between the insulation layers of the cable joint, and, in general, leads to lower values of the electric field and, in particular, to lower maximum values. This is beneficial for reducing the phenomena of space charge injection, partial discharges and a premature ageing of the insulation layers of the cable joint. This also supports the other part of Hypothesis H4 that was left unanswered in the previous Chapter, respectively that improving cable joint design (by incorporating a FGM layer) has a positive effect on both the reduction of space charge as well as its effects.

Chapter 9. General conclusions. Contributions. Perspectives

9.1. Conclusions

1. The analysis of the degradation of the insulation of DC cable joints (XLPE, EPR, EPDM) by FTIR shows that, under the action of heat, their molecules fracture and / or interact with oxygen, leading to the appearance of polar and / or electrically charged by-products; higher residual compounds for EPR and higher number of oxidized groups for EPDM;
2. The values of the electrical conductivity decrease with the measurement duration and increase with the electric field and with the measurement temperature. The increase of the values of T and E leads to the increase of the electrical conductivity of all samples, both unaged and aged (and more for EPR than for EPDM or XLPE);
3. The increase of the ageing time for the samples determines an increase of the electrical conductivity values for all the samples (more for EPR than for EPDM);
4. The use of the empirical relation proposed in the thesis for the calculation of the electrical conductivity according to the values of T and E allows obtaining values of electrical conductivity close to those determined experimentally;
5. The permittivity values decrease with the ageing time for the XLPE and EPDM samples and increase for the EPR samples. These variations are, expressed in percentage, smaller than those of the electrical conductivity;
6. The values of the relaxation time (τ) of the space charge depend on the nature of the samples, on their state, the temperature and the applied electric field. For unaged flat samples subjected to an applied electric field of 1 kV/mm for 3600 s, τ has higher values for XLPE (125 400 s) than for EPDM (6310 s) and EPR (4760 s), and its values decrease with the ageing time: for XLPE about 6 times (to 22 000 s) and for EPR about 3 times (to 1590 s). τ increases with the measurement temperature and the applied electric field;
7. A volume charge density was present in all samples. Its distribution in space depends on the nature of the sample, on the value and the method of applying the voltage, the ageing state, etc. The highest values of the space charge density ρ_v are obtained for the EPR samples, followed by the EPDM and the XLPE samples;
8. The increase of the applied voltage value leads to the increase of the space charge density values, the highest increases obtained for EPR , followed by EPDM and XLPE.
9. The increase of the ageing time leads, initially, to the decrease of $\rho_{v,avg}$ for XLPE and EPR flat samples (after the first 30 days), followed by an increase (until the end of the ageing period), and leads to an increase of $\rho_{v,avg}$ for EPDM and XLPE / EPR samples;
10. The space charge density accumulated in the sample also depends on the method of manufacturing. For cylindrical EPR / XLPE samples manufactured using triple-extrusion, $\rho_{v,avg}$ is lower (0.15 C/m^3 for an applied electric field of 10 kV/mm) than in the case of flat EPR / XLPE samples (or also flat EPDM / XLPE samples) manufactured by pressing with a laboratory press (1.6 C/m^3 for an applied electric field of 10 kV/mm);
11. The accumulation of space charge leads to local intensification of the electric field in all samples. E becomes, locally, up to 4 times more intense in XLPE in the case of XLPE / EPR samples and up to 1.25 times in XLPE in the case of XLPE / EPDM samples. For of XLPE / EPR samples, the increase of the residual charge density $\rho_{v,avg}$ with E_{app} (between 5 and 15 kV/mm) from 1.0 to 3.7 C/m^3 is correlated with an increase of the maximum value of the electric field in the sample of 3.75 times (from 20 to 75 kV/mm). For XLPE / EPDM samples, the increase of the value of $\rho_{v,avg}$ from 0.45 to 1.00 C/m^3 with the applied electric field (between 5 and 15 kV/mm) is correlated with an increase of the maximum value of the electric field in the sample of 1.85 times (from 19 to 35 kV/mm);

12. In the case of multi-layered samples (flat and cylindrical), apart from the volume charge density, at the interfaces between their homogeneous areas a surface charge density is separated. The higher the electrical conductivity of the second component of the sample (the first is XLPE), the faster the surface charge density accumulates, and the higher is its maximum value ($\rho_{s,max}$). Thus, at an applied electric field of 10 kV/mm, for unaged flat samples of XLPE / EPR the value for the maximum surface charge density was $\rho_{s,max} = -3.5\ \mu C/m^2$ and for XLPE / EPDM was only $\rho_{s,max} = -0.75\ \mu C/m^2$;
13. For higher temperatures and more intense electric fields, the accumulation of the surface space charge is faster, and its density ρ_s varies with T and E. The variations of ρ_s with the temperature are more pronounced than the variations with the electric field;
14. In the presence of the applied voltage, the values of E decrease in the vicinity of the electrodes and increase in the central areas of the samples. When the voltage is removed, the values of E are reduced in time, but they are not cancelled even after one hour;
15. The incorporation of a FGM layer in DC cable joints leads to a lower accumulation of space charge at the interfaces between the insulation layers of the cable joint and, in general, leads to lower values for the electric field and, in particular, to lower maximum values. This is beneficial for reducing the phenomena of space charge injection, partial discharges and premature ageing of the insulation layers of the cable joint;
16. Insulation materials used for the insulation layers of DC cable joints must have the lowest possible value of accumulated space charge in their operation. For this, the degree of purity of the basic materials and of the manufacturing technology must be improved and materials with smaller variations of ρ_v and, implicitly, of $\rho_{v,avg}$ must be used;
17. From the analysis of all the results regarding the accumulation of space charge and the computation of the electric field in the aged samples it results that, between EPR and EPDM, for the realization of cable joints it would be preferable to use EPDM;
18. Hypotheses H1, H2, H3 and H4 have been confirmed.

9.2. Personal contributions

1. Realization of procedures for manufacturing flat samples of XLPE, EPR and EPDM, as homogeneous as possible and with thicknesses as constant as possible;
2. Realization of an efficient procedure for manufacturing XLPE / EPR and XLPE / EPDM flat multi-layered samples from flat samples, with high quality surfaces and interfaces;
3. Determination of the thickness of the interface layer of XLPE / EPR multi-layered unaged flat samples through scanning electron microscopy ($g \approx 0.5\ \mu m$);
4. Realization of an experimental study (through FTIR) concerning the effects of accelerated thermal ageing on XLPE, EPR and EPDM samples;
5. Realization of an experimental study concerning the variation of electrical conductivity and relative permittivity of XLPE, EPR, EPDM, XLPE / EPR and XLPE / EPDM flat samples with the applied voltage, measurement temperature and the ageing time;
6. Realization of an electrical conductivity measurement cell for flat samples, capable of determining the electrical conductivity in a wide range of measurement temperatures (from 20 up to 90 °C) and applied voltages (from 0.1 up to 30 kV);
7. Proposing a new empirical expression for the computation of the electrical conductivity, depending on the temperature (T = 30 – 70 °C) and the electric field (E = 1 – 30 kV/mm);
8. Realization of an experimental study concerning the variation of the values of the space charge density with the applied electric field and the ageing state for XLPE, EPR, EPDM, XLPE / EPR and XLPE / EPDM samples, and with the applied voltage for EPR / XLPE cylindrical samples;
9. Improving the software applications for the acquisition and the processing of the electrical signal used for the experimental determination of the space charge density;

10. Realization of a theoretical study on the influence of the electrical voltage and temperature on the surface charge density accumulated at the interfaces of multi-layered flat and cylindrical samples;
11. Realization of a theoretical study on the influence of the volume charge density and the surface charge density on the electric field for multi-layered flat and cylindrical samples;
12. Realization of a theoretical study on the influence of FGM layer and cavities on the electric field and the space charge distributions in the insulation layers of DC cable joints;
13. Determining the effects of space charge (distributed in volume and, in the case of multi-layered samples, also on surfaces) on the distribution of the electric field in DC cable joints insulations and proposing methods to reduce the space charge;

9.3. Perspectives

1. Improving the technological process of manufacturing samples and DC cable joints in order to reduce the space charge, respectively reducing the concentrations of technological products, impurities, degradation products, etc.;
2. Study of the influence of the polyethylene terephthalate (PET) layer used in the manufacturing of samples on the values of electrical conductivity and space charge;
3. Study of the variation of electrical conductivity with measurement temperature, applied voltage and ageing state for insulation materials used in cable joints by using semiconductor electrodes, because the type of electrode – insulator interface influences the injection of charge carriers and thus the electrical conductivity of the sample;
4. Study of the variation of the relative permittivity at low frequencies (close to DC) on the accumulation of space charge (in DC);
5. Study of the variation of the space charge density with the measurement temperature, applied voltage and ageing state for the insulation materials used in the cable joints by using semiconductor electrodes;
6. Study of the variation of the accumulation of space charge at temperatures higher than 30 °C and, possibly, under a temperature gradient;
7. Study of the effects of thermal + electrical + mechanical multifactor ageing on the properties of cable joints insulation materials and on the accumulation of space charge;
8. Study of the influence of the period of storage (elapsed time between the end of accelerated ageing and measurement) of aged samples on the values of space charge;
9. Performing tests to measure the space charge density on real cable joints with an insulation between the cable and the joint of XLPE / EPR and XLPE / EPDM, to confirm the results obtained on flat and cylindrical samples;

References

[15] G. C. Montanari and P. Seri, “HVDC and UHVDC polymeric cables: Feasibility and material development”, IEEE Electr. Insul. Mag., vol. 35, no. 5, pp. 28–35, Sep. 2019

[16] P. Bergelin et al., “640 kV extruded HVDC cable systems - NKT”

[19] IEA, “World Energy Outlook 2017”, last revision Dec 2019

[30] G. Mazzanti et al., “The insulation of HVDC extruded cable system joints. Part 1: Review of materials, design and testing procedures”, IEEE Trans. Dielectr. Electr. Insul., vol. 26, no. 3, pp. 964–972, 2019

[34] M. Albertini et al., “Development and high temperature qualification of innovative 320 kV DC cable with superiorly stable insulation system”, in 9th Inter. Conf. on Insulated Power Cables (Jicable), 2015, pp. 15–21

[40] CIGRE Technical Brochure 177, “Accessories for HV cables with extruded insulation”, 2001

[46] G. Mazzanti and M. Marzinotto, “Extruded cables for high-voltage direct-current transmission : Advances in research and development”. IEEE Press, 2013

[57] “IEEE Recommended Practice for Space Charge Measurements on High-Voltage Direct-Current Extruded Cables for Rated Voltages up to 550 kV”, 1732, 2017

[62] K. S. Suh et al., “Interfacial properties of XLPE/EPDM laminates”, IEEE Trans. Dielectr. Electr. Insul., vol. 7, no. 2, pp. 216–221, Apr. 2000

[73] G. Mazzanti and M. Marzinotto, “Advanced electro-thermal life and reliability model for high voltage cable systems including accessories”, IEEE Electr. Insul. Mag., vol. 33, no. 3, pp. 17 25, 2017

[92] TE Connectivity, “Raychem High Voltage Cable Accessories up to 245 kV” [Online].

[103] “A method of manufacturing a high-voltage DC cable joint, and a high-voltage DC cable joint”, EP3034561A1, P. Meier et al., 2019

[132] “Evaluation and qualification of electrical insulation systems”, IEC 60505, 2011

[172] C. Blivet et al., “Thermal oxidation of cross-linked PE and EPR used as insulation materials: Multi-scale correlation over a wide range of temperatures”, Polym. Test., vol. 93, Jan. 2021

[174] Takashi Suenaga et al., “Effect of antioxidants on thermal degradation of EPDM and XLPE”, in 2008 International Conference on Condition Monitoring and Diagnosis, 2008, pp. 294–298

[200] M. Ieda, “Electrical Conduction and Carrier Traps in Polymeric Materials”, IEEE Trans. Electr. Insul., vol. EI-19, no. 3, pp. 162–178, Jun. 1984

[231] IEEE, “IEEE Std 539-2005 IEEE Standard Definitions of Terms Relating to Corona and Field Effects of Overhead Power Lines”, IEEE Std 539-2005 (Revision of IEEE Std 539-1990), 2005

[246] R. Men et al., “Effect of thermal ageing on space charge in ethylene propylene rubber at DC voltage”, IEEE Trans. Dielectr. Electr. Insul., vol. 26, no. 3, pp. 792–800, Jun. 2019

[247] G. C. Montanari and L. Simoni, “Aging phenomenology and modeling”, IEEE Trans. Electr. Insul., vol. 28, no. 5, pp. 755–776, 1993

[252] G. Mazzanti et al., “A protocol for space charge measurements in full-size HVDC extruded cables”, IEEE Trans. Dielectr. Electr. Insul., vol. 22, no. 1, pp. 21–34, Feb. 2015

[261] G. C. Montanari, “The electrical degradation threshold of polyethylene investigated by space charge and conduction current measurements”, IEEE Trans. Dielectr. Electr. Insul., vol. 7, no. 3, pp. 309–315, 2000

[262] C. Stancu et al., “PN-II-RU-TE-2014-4-0280, Report 1: Manufacture of multi-layer joints planar models”, 2015

[265] J.-P. Crine et al., “Oxidation and thermal resistance of HMW-PE and XLPE HV”, Conf. Record of the 1998 IEEE Int. Symp. on El. Insul., pp. 219–224, 1998

[268] G. Rizzo et al., “Review of the PEA Method for Space Charge Measurements on HVDC Cables and Mini-Cables”, Energies, vol. 12, no. 18, p. 3512, Sep. 2019

[272] J. C. M. Suarez et al., “Study of the effect of gamma irradiation on polyolefins-low-density polyethylene”, Polym. Degrad. Stab., vol. 75, no. 1, pp. 143–151, Jan. 2002

[273] J. P. Crine et al., “A Critical Evaluation of Analytical Techniques for the Characterization of Extruded Dielectric Cables”, IEEE Trans. Electr. Insul., vol. 26, no. 1, pp. 131–139, 1991

[274] Y. Liu and X. Wang, “Research on property variation of silicone rubber and EPDM rubber under interfacial multi-stresses”, IEEE Trans. Dielectr. Electr. Insul., vol. 26, no. 6, pp. 2027–2035, Dec. 2019

[275] I. Plesa et al., “Properties of Polymer Composites Used in High-Voltage Applications”, Polymers (Basel)., vol. 8, no. 5, pp. 1–73, 2016

[278] Y. Kemari et al., “Correlations between structural changes and dielectric behavior of thermally aged XLPE”, IEEE Trans. Dielectr. Electr. Insul., vol. 26, no. 6, pp. 1859–1866, Dec. 2019

[280] A. Sriraman et al., “Dielectric and Mechanical Behavior of Thermally Aged EPR/CPE Cable Materials”, in Annual Report - Conference on Electrical Insulation and Dielectric Phenomena, CEIDP, 2018, pp. 598-601

[281] R. M. Eichhorn, “A critical comparison of XLPE and EPR for use as electrical insulation on underground power cables”, IEEE Transactions on Electrical Insulation, vol. EI-16, no. 6. pp. 469–482, 1981

[294] M. Abou-Dakka et al., “Space charge evolution in XLPE and EPR under high uniform electric fields”, in Conference on Electrical Insulation and Dielectric Phenomena (CEIDP), 1998, vol. 1, pp. 136-139

[295] R. Men et al., “Space charge properties of EPDM under different electric field and thermal ageing”, in 10th International Conference on Insulated Power Cables, 2019, pp. C4-3

[300] “Method of forming a flexible joint with resistive field grading material for HVDC cables”, US8578602B2, C. Thomas, 2013